USGS
science for a changing world

Significance of a Near-Source Tephra-Stratigraphic Sequence to the Eruptive History of Hayes Volcano, South-Central Alaska

Scientific Investigations Report 2014–5133

U.S. Department of the Interior
U.S. Geological Survey

FRONT COVER
Portion of the Hayes River outcrop 31 km northeast of Hayes Volcano, along the Hayes River immediately downstream from the terminus of Hayes Glacier. Photograph by Andrew Calvert, 2011.

Significance of a Near-Source Tephra-Stratigraphic Sequence to the Eruptive History of Hayes Volcano, South-Central Alaska

By Kristi L. Wallace, Michelle L. Coombs, Leslie A. Hayden, and Christopher F. Waythomas

Scientific Investigations Report 2014–5133

U.S. Department of the Interior
U.S. Geological Survey

U.S. Department of the Interior
SALLY JEWELL, Secretary

U.S. Geological Survey
Suzette M. Kimball, Acting Director

U.S. Geological Survey, Reston, Virginia: 2014

Suggested citation:
Wallace, K.L., Coombs, M.L., Hayden, L.A., and Waythomas, C.F., 2014, Significance of a near-source tephra-stratigraphic sequence to the eruptive history of Hayes Volcano, south-central Alaska: U.S. Geological Survey Scientific Investigations Report 2014-5133, 32 p., *http://dx.doi.org/10.3133/sir20145133*.

ISSN 2328-0328 (online)

Acknowledgments

We would like to thank Thomas Sisson, U.S. Geological Survey for kindly sharing pumice sample analyses. We would also like to thank Josh Ruether, University of Alaska, Fairbanks for providing archeological reports and theses on Susitna River valley tephras. We thank Charlie Bacon and Jorge Vazquez, U.S. Geological Survey, for providing constructive reviews that improved the manuscript.

Contents

Abstract....1
Introduction....1
Study Methods....3
Results....7
- Field Descriptions and Stratigraphy....7
  - Unit I: Hayes River Ignimbrite....7
  - Unit II: Flowage and Bouldery Diamicton Package....7
  - Unit III: Tephra-Fall Sequence....7
- Sample Descriptions....12
  - Units I and II: Hayes River Ignimbrite and Flowage/Diamicton Package....12
  - Unit III: Tephra-Fall Sequence....12
  - Other Samples....18
- Whole Rock Compositions....18
- Phase Compositions....20
  - Groundmass Glass....20
  - Fe-Ti Oxides....20
  - Amphibole....23
  - Biotite....23

Significance of Sample Analyses to Eruptive History of Hayes Volcano....24
- Hayes River Exposure....24
- Correlation to Previously Described Hayes Volcano Deposits....27
  - Section 23 of Riehle (1985)....29
  - Jarvis, Tangle Lakes, and Cantwell Tephra Deposits....29
  - Southeastern Lobe of Hayes Tephra Set H....29
  - Oshetna Tephra....29
  - Other Regional Tephras Possibly Correlated to Hayes Volcano....30
  - Possible Regional Correlatives to the Hayes River Ignimbrite....30

Concluding Remarks....30
References Cited....30

Figures

1. Location of Hayes Volcano in south-central Alaska and outcrops containing known or suspected deposits of Hayes tephra set H....2
2. Photograph showing a portion of the Hayes River outcrop at site 11HYKLW001....3
3. Schematic stratigraphic section of the Hayes River outcrop....8
4. Photographs showing characteristics of Units I and II at the Hayes River outcrop....8
5. Stratigraphy of Unit III tephra-fall sequence at the Hayes River outcrop....9
6. Photographs of Unit III, Hayes River outcrop, showing main tephra layers....10
7. Back-scattered electron micrographs of samples from the Hayes River outcrop, Hayes lava dome, and lahar deposit from site 00CW203....13
8. Ternary diagram showing proportions of dominant mafic minerals in Hayes Volcano tephras, as determined by point counts of grain mounts....17
9. Variation diagram showing whole-rock composition of pumiceous clasts erupted from Hayes Volcano compared to those from nearby volcanoes in south-central Alaska....19
10. Silica variation diagrams for groundmass glass of pumiceous deposits within the Hayes River outcrop and other similar published data attributed to a Hayes Volcano source.21
11. Magnetite and ilmenite compositions for Hayes River outcrop and other Hayes Volcano samples....22
12. Minor-element variation diagrams for magnetite crystals from dacitic tephras from the Hayes River outcrop and dome sample 99CW1-1....23
13. Alumina concentrations of amphibole phenocrysts from Hayes Volcano eruptive products, sorted by deposit....24
14. Variation diagrams showing amphibole spot analyses for eruptive products of Hayes Volcano....25
15. Biotite compositions for eruptive products of Hayes Volcano. Each point represents an average of multiple analyses on a single crystal....26
16. Overview of distinctive features, of and possible correlatives to, the Hayes River outcrop tephra-fall deposits of Unit III....28

Tables

[Table 4, 6–9 available online only at http://pubs.usgs.gov/sir/2014/5133/.]

1. Type of analyses completed for samples of Hayes River outcrop, in stratigraphic order....4
2. Radiocarbon ages from Hayes River outcrop Unit III/tephra-fall sequence....10
3. Descriptions of Unit III tephra-fall deposits from the Hayes River outcrop....11
5. Major-element glass compositions from Hayes River outcrop, determined by electron probe microanalyzer at the U.S. Geological Survey in Menlo Park, Calif....16

Appendixes

[Available online only at http://pubs.usgs.gov/sir/2014/5133/.]

A. Point and normalized major-element glass compositions from Hayes River outcrop Units I and III, determined by electron probe microanalyzer at the U.S. Geological Survey in Menlo Park, Calif.

B. Magnetite and ilmenite spot compositions, determined by electron probe microanalyzer at the U.S. Geological Survey in Menlo Park, Calif.

C. Biotite point compositions, determined by electron probe microanalyzer at the U.S. Geological Survey in Menlo Park, Calif.

Conversion Factors

SI to Inch/Pound

Multiply	By	To obtain
	Length	
micrometer (um)	0.00003937	inch (in.)
millimeter (mm)	0.03937	inch (in.)
centimeter (cm)	0.3937	inch (in.)
meter (m)	3.281	foot (ft)
kilometer (km)	0.6214	mile (mi)
meter (m)	1.094	yard (yd)

Horizontal coordinate information is referenced North American Datum of 1983 (NAD 83)

Altitude, as used in this report, refers to distance above sea level.

Abbreviations and Symbols

ADGGS	Alaska Division of Geological and Geophysical Surveys
AK	Alaska
Aj/Cox	Incipiently developed A horizon/oxidized C horizon
amph.	amphibole
AT-#	Alaska Tephra Laboratory identification number
AVO	Alaska Volcano Observatory
B.P.	before present, radiocarbon years before 1950
^{14}C	radiocarbon
°C	degrees celcius
CA	coarse ash (1/2–1 mm)
CL	coarse lapilli (16–64 mm)
cal	calibrated
Calif.	California
commun.	communication
cm	centimeter
EPMA	electron probe microanalyzer
FA	fine ash (<1/8–1/4 mm in diameter)
FL	fine lapilli (2–4 mm)
Hbl.	hornblende
HD	Hayes dome
ICP-MS	inductively coupled plasma-mass spectometery
ID	identification
ka	thousand years ago
km	kilometers
m	meters
MA	medium ash (1/2–1/4 mm in diameter)
ML	medium lapilli (4–16 mm)
µm	micron
n/a	not applicable
ppm	parts per million
pop.	population (glass)
VFA	very fine ash (1/16–1/8 mm in diameter)
WR	whole rock
WSU	Washington State University
wt.%	weight percent
s	seconds
UAF	University of Alaska Fairbanks
USGS	U.S. Geological Survey
XRF	x-ray flouresence
yr	years
‰	per mil
#	number

Significance of a Near-Source Tephra-Stratigraphic Sequence to the Eruptive History of Hayes Volcano, South-Central Alaska

By Kristi L. Wallace, Michelle L. Coombs, Leslie A. Hayden, and Christopher F. Waythomas

Abstract

Bluffs along the Hayes River valley, 31 km northeast and 40 km downstream from Hayes Volcano, reveal volcanic deposits that shed new light on its eruptive history. Three thick (>10 cm) and five thin (<10 cm) tephra-fall deposits are dacitic in whole rock composition and contain high proportions of amphibole to pyroxene and minor biotite and broadly correlate to Hayes tephra set H defined by earlier investigators. Two basal ages for the tephra-fall sequence of 3,690±30 and 3,750±30 ^{14}C yr B.P. are also consistent with the Hayes tephra set H timeframe. Distinguishing among Hayes tephra set H units is critical because the set is an important time-stratigraphic marker in south-central Alaska and this section provides a new reference section for Hayes tephra set H. Analysis of Fe-Ti oxide grains in the tephras shows promise for identifying individual Hayes deposits. Beneath the dacitic tephra sequence lies an older, poorly sorted tephra (tephra A) that contains dacite and rhyolite lapilli and whose basal age is 4,450±30 ^{14}C yr B.P. Immediately below the tephra-fall sequence (Unit III) lies a series of mass-flow deposits that are rich in rhyodacitic clasts (Unit II). Below Unit II and possibly coeval with it, is a 20–30 m thick pumiceous pyroclastic-flow deposit (Unit I) that extends to the valley floor. Here informally named the Hayes River ignimbrite, this deposit contains pumice clasts of rhyolite with quartz, sanidine, plagioclase, and biotite phenocrysts, an assemblage that is unique among known Quaternary volcanic products of Hayes and other Alaskan volcanoes. Units I, II, and tephra A of Unit III represent at least two previously unrecognized eruptions of Hayes Volcano that occurred prior to ~3,700 yr B.P. No compositionally equivalent distal tephra deposits correlative with Hayes Volcano rhyodacites or rhyolites have yet been identified, perhaps indicating that some of these deposits are pre-Holocene, and were largely removed by glacial ice during the last ice age. More field and analytical work is needed to further refine the eruptive history of Hayes Volcano.

Introduction

Hayes Volcano is a snow- and ice-covered volcano in the northern Tordrillo Mountains, 140 km northwest of Anchorage, Alaska (fig. 1). The northernmost active volcano in the Aleutian-Alaskan volcanic arc, it was discovered in 1975 (Miller and Smith, 1976), and little is known about its eruptive history owing to the limited exposure of volcanic deposits. It has produced pyroclastic flows that descended into the Hayes River drainage, lahars that travelled down the Hayes River and into the Skwentna River (Waythomas and Miller, 2002), and most notably, a series of seven or eight closely spaced tephra-fall deposits between ~3,800–3,500 ^{14}C yr B.P. (Riehle, 1985, 1994; Riehle and others, 1990; Begét and others, 1991). These tephra-fall deposits, informally known as "Hayes tephra set H" (herein refered to as tephra set H), are the most widespread tephras of Holocene age in south-central Alaska (Riehle, 1994). The tephra set has a composite volume of about 10 km^3 and is distributed as far as 650 km north, south, and east of Hayes Volcano.

Tephras within tephra set H, as described by Riehle (1985) and Riehle and others (1990), are dacitic in composition, and contain rhyolitic glass and phenocrysts of plagioclase, amphibole, pyroxene, Fe–Ti oxides, and rare biotite. The high proportion of amphibole and trace amounts of biotite distinguish tephra set H tephras from other Holocene tephras erupted from Cook Inlet volcanoes south of Hayes (Spurr, Redoubt, Iliamna, and Augustine) (Riehle, 1985). Tephras from locations as widespread as the Kenai Peninsula (Combellick and Pinney, 1995; de Fontaine and others, 2007), Denali National Park (Child and others, 1998), the Susitna River valley (Dixon and Smith, 1990), and the Matanuska River valley (Fontana, 1988), have been correlated to tephra set H on the basis of mineralogy, major-element glass composition, and age. Begét and others (1991) recognized that the Jarvis Ash Bed and informal Cantwell and Tangle Lakes tephra deposits of interior Alaska, all likely formed during a single eruption during the tephra set H sequence. Tephras of tephra set H are present in the Anchorage area, and are the only tephras of Holocene age of any substantial thickness (as much as 2 cm) in and around Alaska's most populated city (Riehle, 1985). Some ambiguity remains, however, regarding exactly how many eruptions occurred during the interval of time represented by the tephra set, and delineation of discrete deposits within the set awaits further work.

Aside from tephra set H, evidence for other Holocene eruptions of Hayes Volcano is sparse (Waythomas and Miller, 2002). Riehle (1985) describes a possible Hayes tephra that

is ~500–1,000 ^{14}C yr B.P. Additionally, archeological studies in the upper Susitna River valley revealed an older regional tephra deposit, informally named the Oshetna tephra (Child and others, 1998), that was erupted 5,790–5,960 ^{14}C yr B.P. and has been attributed to Hayes Volcano (J.E. Dixon and others, written commun(s)., 1985; Dilley, 1988; Dixon and Smith, 1990). A younger, fine ash bed informally known as the Devil tephra, also found throughout the upper Susitna River valley, was erupted 1,420–1,516 ^{14}C yr B.P. and is also a likely product of Hayes Volcano (Dixon and Smith, 1990). Only a few samples have been collected from the volcano itself, and none have been radiometrically dated.

In this report, we describe a stratigraphic section 31 km northeast of Hayes Volcano, along the Hayes River immediately downstream from the terminus of the Hayes Glacier (fig. 1*B*). This section, referred to as the Hayes River outcrop (fig. 2), is significant because it contains a well-preserved sequence of dacite tephra deposits that generally correlates to tephra set H of Riehle and others (1990), but that also includes at least one additional tephra-fall deposit dated at 4,450±30 ^{14}C yr B.P. that is significantly different in composition. This tephra records an eruption of Hayes Volcano that occurred prior to the eruption of tephra set H. Lower in the section, the Hayes River outcrop contains an older rhyodacite-bearing flowage

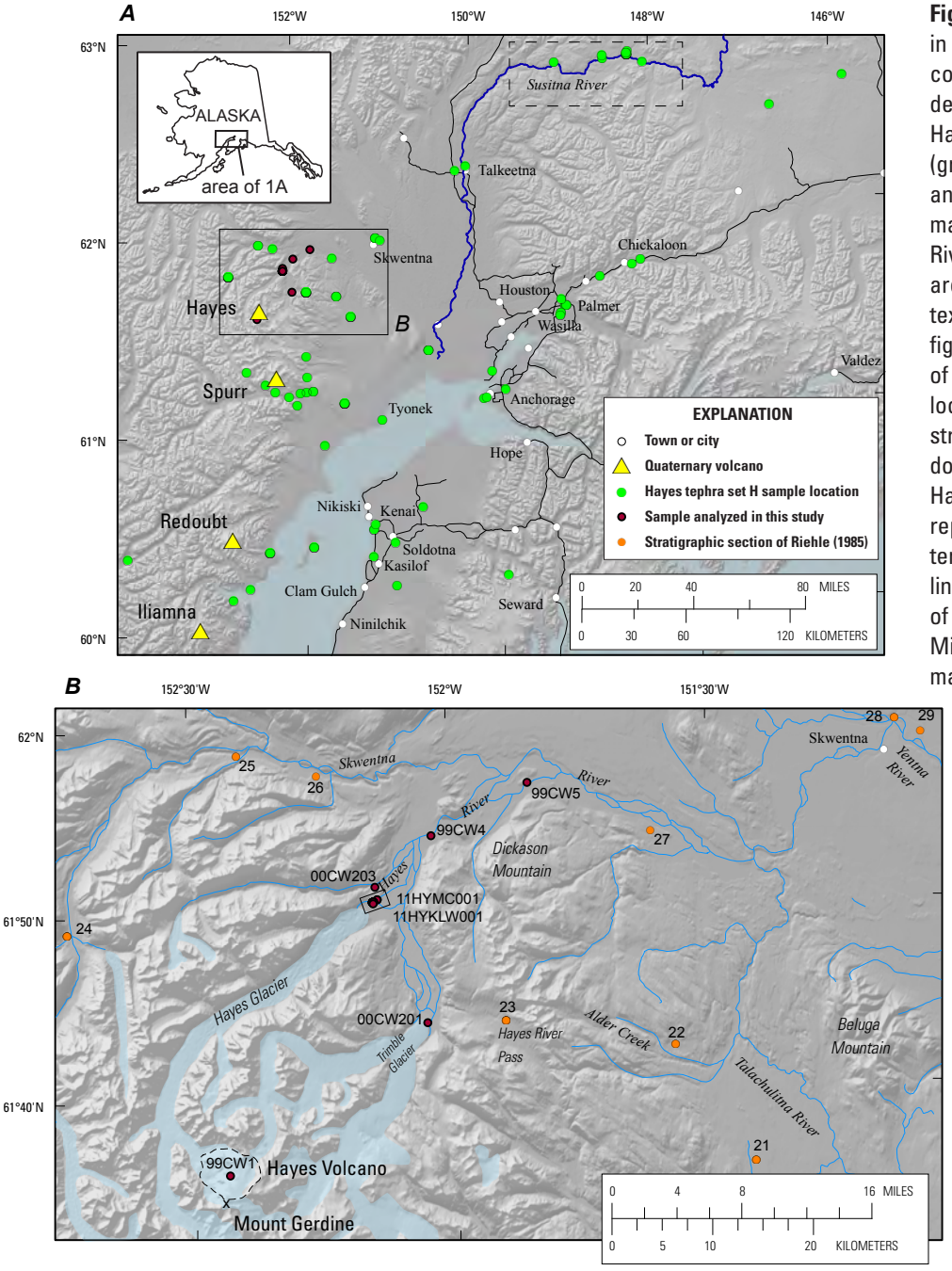

Figure 1. Location of Hayes Volcano in south-central Alaska and outcrops containing known or suspected deposits of Hayes tephra set H. *A*, Hayes tephra set H sample locations (green dots). Locations of samples analyzed in this study (red dots), major roads (black lines), and Susitna River (blue line). Area of 1979–85 archeological studies, as discussed in text, is shown by dashed box. Area of figure 1*B* shown by black box. *B*, Map of the Hayes Volcano area showing location of samples (red dots) and stratigraphic section locations (orange dots) of Riehle (1985). Location of the Hayes River outcrop discussed in this report shown by black rectangle near terminus of Hayes Glacier. Dashed line is generalized extent of the edifice of Hayes Volcano (Waythomas and Miller, 2002). Generalized extent of major glaciers shown in blue.

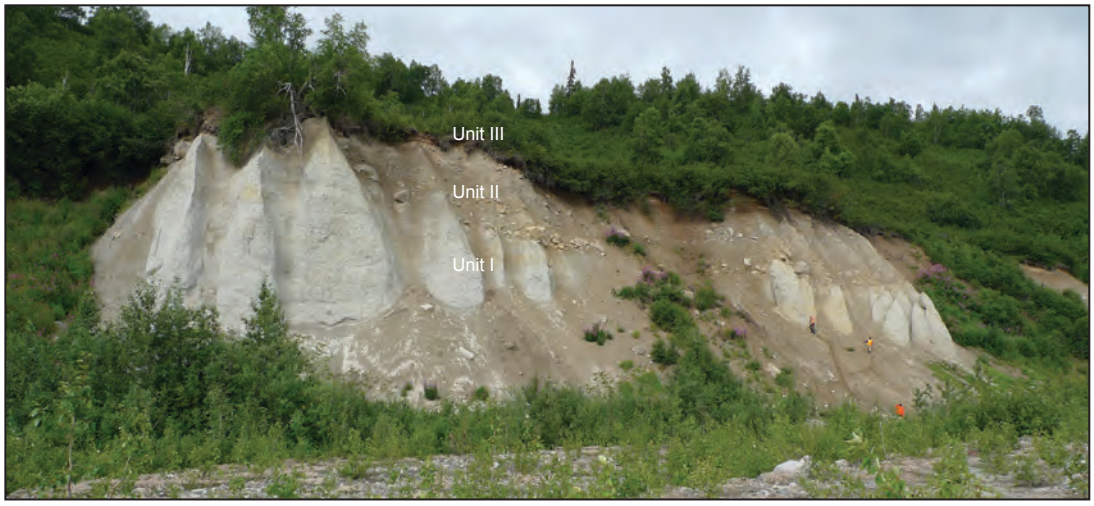

Figure 2. Photograph showing a portion of the Hayes River outcrop at site 11HYKLW001, 31 km northeast of Hayes Volcano, along the Hayes River immediately downstream from the terminus of the Hayes Glacier. People in photograph for scale ~1.5 m tall. Major units (I, II, and III) are labelled.

and diamicton package (fig. 2). The most prominent deposit, exposed at the bluff's base, is a pumiceous pyroclastic-flow deposit that is >20 m thick, here informally named the Hayes River ignimbrite. The Hayes River ignimbrite is rhyolitic in bulk composition, with mineralogy and chemistry distinct from the known dacitic tephras of tephra set H and the rhyodacite clasts contained within the overlying flowage and diamicton package. This unit represents a significant eruption of Hayes Volcano prior to 4,450±30 ^{14}C yr B.P.

In addition to the stratigraphic relations described above, we report new data on whole-rock (WR), glass, and mineral compositions from the major units present at the Hayes River outcrop (fig. 2), as well as from samples of lava domes on the Hayes edifice and juvenile clasts from lahar deposits along the Hayes River collected in 1999 and 2000 (table 1). In addition, we present three new ^{14}C dates on buried soils related to the Hayes River tephra sequence, and proportions of mafic minerals within each tephra layer. This report provides new information on Holocene eruptive products of Hayes Volcano that will improve correlation to regional Hayes Volcano tephra deposits, and also illustrates that further work is needed to better define the volcano's eruptive history.

Study Methods

The Hayes River outcrop (61.84323°N, 152.14522°W) was reached by helicopter and samples were collected in August and September 2011. Several samples described here also were collected in 1999 and 2000.

Major and trace-element compositions of 20 samples were determined at the Washington State University (WSU) Geoanalytical Laboratory using x-ray fluorescence (XRF) and inductively coupled plasma-mass spectrometry (ICP-MS) techniques (table 1). Samples were cleaned using tap water in a sonication bath and dried for 48 hours at 60 °C prior to analysis. For coarse deposits, a single lapillus or lava chunk was analyzed; for tephra samples, multiple similar, representative lapilli were hand-picked and ground for a single analysis. XRF and ICP-MS analyses were performed following the methods of Johnson and others (1999) and Knaack and others, written commun. (1994). All intensity values were reduced using a single calibration file to decrease interbatch analytical variations.

Because of the relatively proximal nature of the deposits to Hayes Volcano, we were able to separate out individual fine lapilli and mount 10–20 per sample for glass and mineral analyses. In addition, coarse lapilli from samples AT-2558 (tephra A) and AT-2560 (tephra F) were impregnated and prepared as polished thin sections. Lapilli mounts, as opposed to fine-grained glass and mineral separates, allowed for petrographic description of the tephras, as well as determination of homogeneity of glass and mineral compositions on a lapillus-by-lapillus basis.

Back-scattered electron images of thin sections of representative components were acquired using the U.S. Geological Survey (USGS) JEOL JSM-6510LV scanning electron microscope in Anchorage, Alaska. The same mounts were used for both back-scatter and electron microprobe analyses.

Major-element glass and mineral analyses were conducted using wavelength dispersive techniques with a 5-spectrometer JEOL 8900R electron probe microanalyzer (EPMA) at the USGS in Menlo Park, Calif. Concentrations were determined with the CIT-ZAF reduction scheme (Armstrong, 1995). Glass analyses used a 5-µm-diameter beam with 5 nA current and 15 kV accelerating potential. Reported glass compositions are the averages of 10–25 spot analyses or fewer if multiple populations were found within a single sample; background intensities were determined 1–3 times for each grain. Count times were 10 s for Na (which was analyzed first to reduce Na-loss), 10 s for S and Cl , and 30 s for all other elements. During analysis, sets of 5–10 replicate analyses of glass standards RLS-132, RLS-75, and GSC (Jarosewich and others, 1979) were performed to monitor instrument drift. Natural glass and mineral standards were used for calibration: RLS-132 for Si; basaltic glass VG2 for Fe, Mg, and Ca; Orthoclase 1 for K and Al; Tiburon albite for Na; Mn_2O_3 for Mn; TiO_2 for Ti; sodalite for Cl; and

Table 1. Type of analyses completed for samples of Hayes River outcrop, in stratigraphic order.

[Grain-size terms from White and Houghton, 2006. VFA, very fine ash (1/16–1/8 mm); FA, fine ash (<1/8–1/4 mm); MA, medium ash (1/2–1/4 mm); CA, coarse ash (1/2–1 mm); FL, fine lapilli (2–4 mm); ML, medium lapilli (4–16 mm); CL, coarse lapilli (16–64 mm). ID, identification; km, kilometers; cm, centimeters; mm, millimeters; n/a, not applicable]

Sample name	Tephra Lab ID[a]	Latitude (NAD83)	Longtitude (NAD83)	Unit[b]	Description	Pumice color	Pumice Munsell color[c]	Glass	Whole-rock	Oxides	Amphibole	Biotite
Unit III: Tephra-Fall Sequence												
11HYKLW001-11	AT-2564	61.84323	-152.14522	Unit III: tephra H2	Upper 10 cm of 20 cm dark yellowish/orange, normally graded VFA-FL fallout.	white oxidized	10YR 7/4	x		x	x	
11HYKLW001-10	AT-2563	61.84323	-152.14522	Unit III: tephra H1	Lower 10 cm of 20 cm dark yellowish orange normally graded VFA-ML fallout.	white oxidized	10YR 7/4	x		x	x	
11HYKLW001-9	AT-2562	61.84323	-152.14522	Unit III: tephra G	5 cm normal graded, medium gray MA-FL fallout.	cream white	10YR 8/2	x		x	x	
11HYKLW001-8	AT-2561	61.84323	-152.14522	Unit III: tephra F2	Upper 27 cm of 37 cm very pale orange, massive CA-FL fallout.	cream white	10YR 8/2	x		x	x	
11HYKLW001-7	AT-2560	61.84323	-152.14522	Unit III: tephra F1	Lower 10 cm of 37 cm very pale orange, normally graded CA-ML fallout.	cream white	10YR 8/2	x	x	x	x	x
11HYKLW001-13	AT-2565	61.84323	-152.14522	Unit III: tephra E	1 cm pale yellowish brown MA-CA fallout.	cream white	10YR 8/2	x		x	x	
11HYKLW001-15	AT-2567	61.84323	-152.14522	Unit III: tephra D	1 cm medium gray, massive CA fallout.	cream white	10YR 8/2	x		x	x	
11HYKLW001-14	AT-2566	61.84323	-152.14522	Unit III	Woody paleosol directly below Unit D tephra-no date	n/a	n/a					
11HYKLW001-17	AT-2568	61.84323	-152.14522	Unit III	Woody paleosol directly below Unit C tephra-no date	n/a	n/a					
11HYKLW001-6	AT-2559	61.84323	-152.14522	Unit III: tephra B	20–25 cm salt & pepper, well-sorted CA fallout.	bright white	N9	x		x	x	
11HYKLW001-2	AT-2555	61.84323	-152.14522	Unit III	Weakly developed paleosol directly below Unit B-3,750+/-30 yr B.P.	n/a	n/a					
11HYKLW001-3	AT-2556	61.84323	-152.14522	Unit III	Prominent well-developed paleosol directly above Unit A-3,690+/-30yr B.P.	n/a	n/a					
11HYKLW001-5	AT-2558	61.84323	-152.14522	Unit III: tephra A	3–5 cm moderate brown, poorly sorted FA-CL fallout.	white-2 types	N9 & 10YR 8/2	x	x	x	x	x
11HYKLW001-4	AT-2557	61.84323	-152.14522	Unit III	Prominent paleosol directly below Unit A-basal age of tephra sequence-4,450+/-30 yr B.P.	n/a	n/a					
Unit II: Flowage and Bouldery Diamicton Package												
11HYMC001-3	n/a	61.84319	-152.1472	Unit II	Dense glassy juvenile clast; dominant clast type in this upper lahar sequence.	bright white	N9		x	x	x	x
11HYMC002-2	n/a	61.84503	-152.13991	Unit II	1-m diameter dense angular crystal-rich juvenile block.	lt. gray	N8		x		x	x

Table 1. Type of analyses completed for samples of Hayes River outcrop, in stratigraphic order. —Continued.

Sample name	Tephra Lab ID[a]	Latitude (NAD83)	Longtitude (NAD83)	Unit[b]	Description	Pumice color	Pumice Munsell color[c]	Glass	Whole-rock	Oxides	Amphibole	Biotite
Unit I: Hayes River ignimbrite (HRI)												
11HYMC002-1	n/a	61.84503	-152.13991	Unit I: HRI	Indurated pumice-bearing ignimbrite clast within boulder breccia near top of HRI.	bright white	N9			x	x	
11HYMC001-4	n/a	61.84319	-152.1472	Unit I: HRI	Quartz-biotite pumice bomb.	bright white	N9		x			x
11HYMC001-5	n/a	61.84319	-152.1472	Unit I: HRI	25x25x10 cm foliated quartz-plagioclase-biotite pumice, friable.	bright white	N9	x	x			
11HYMC001-6	n/a	61.84319	-152.1472	Unit I:HRI	25x25x10 cm foliated quartz-plagioclase-biotite pumice bomb.	bright white	N9		x			x
11HYMC001-7	n/a	61.84319	-152.1472	Unit I: HRI	13x13x9 cm finely vesicular quartz-plagioclase-biotite pumice bomb.	med. gray	N5		x			
11HYMC003-1	n/a	61.84296	-152.14961	Unit I:HRI	Quartz-biotite pumice bomb with notable foliation, friable.	bright white	N9					
11HYMC003-2	n/a	61.84296	-152.14961	Unit I:HRI	Finely vesicular pumice, sturdier than white variety; no foliation, equant vesicles. Same apparent mineralogy. Some banding and gradation between two types.	lt. gray	N7	x	x			
11HYMC003-3	n/a	61.84296	-152.14961	Unit I:HRI	10-cm banded pumice clast.	lt-med. gray	N8-N5					
11HYMC003-4	n/a	61.84296	-152.14961	Unit I:HRI	Dense, 10x5 cm angular block. Bright white matrix encloses abundant phenocrysts of quartz-plagioclase-biotite. Congate inclusion?	bright white	N9		x			x
11HYMC003-5	n/a	61.84296	-152.14961	Unit I:HRI	Dense, 4x5 cm angular block. Bright white matrix encloses abundant phenocrysts of quartz-plagioclase-biotite. Congate inclusion?	bright white	N9		x	x		x
11HYTS001	n/a	61.84319	-152.14720	Unit I:HRI	20-cm diameter quartz-rich pumice bomb.	bright white	N9		x			
11HYTS002	n/a	61.84319	-152.14720	Unit I:HRI	20-cm diameter quartz-rich pumice bomb.	bright white	N9		x			
Other												
00CW201-1	n/a	61.73333	-152.05000	n/a	Tephra fall from near toe of Trimble Glacier.	cream-white	10YR 8/2		x	x		
00CW203-2	AT-190	61.85648	-152.14405	n/a	Dense clast from lahar(?) in small drainage just north of Hayes River outcrop.	bright white	N9		x	x		x

Table 1. Type of analyses completed for samples of Hayes River outcrop, in stratigraphic order. —Continued.

Sample name	Tephra Lab ID[a]	Latitude (NAD83)	Longtitude (NAD83)	Unit[b]	Description	Pumice color	Pumice Munsell color[c]	Glass	Whole-rock	Oxides	Amphibole	Biotite
99CW1-1	AT-197	61.60000	-152.43333	HD	Dome rock from summit area.	very light gray	N8		x		x	x
99CW1-2	n/a	62.60000	-153.43333	HD	Dome rock from summit area.	very light gray	N8		x			
99CW3-3	n/a	61.84167	-152.14833	HRI?	Pumice clast from lahar/pyroclastic flow(?), Hayes River outcrop.	bright white	N9		x			
99CW4-1, <2mm	AT-194	61.90167	-152.03330	n/a	Pumice clast from lahar deposit 8 km downstream of Hayes River outcrop.	cream-white	10YR 8/2		x			
99CW5-2, <2mm	AT-195	61.94667	-151.84533	n/a	Pumice clast from lahar deposit 18 km downstream of Hayes River outcrop	cream-white	10YR 8/2		x			

[a] Alaska Tephra Laboratory and Data Center identification number (AT-#)

[b] Unit refers to stratigraphic unit designation shown in fig. 3, 5: Unit II, rhyodacite-bearing flowage and diamicton; HRI, informal Hayes River ignimbrite; HD, Hayes dome

[c] Munsell colors from Munsell rock color chart; depicts color of pumices when dry

Wilberforce apatite for P. Standard deviations of averages of multiple spot analyses for single unknown samples are generally within those listed above for working standards. Point data for all glass analyses are given in Appendix A.

Analyses of Fe-Ti oxides are mainly of titanomagmatite, but a minority of ilmenite crystals were also analyzed.We used a focus beam for all analyses. During analysis, sets of 4–5 replicate analyses of ilmenite and synthetic $MgAl_2O_4$ were performed to monitor instrument drift. Reported oxide compositions are typically averages of 3–5 spot analyses per crystal, and low standard deviations indicate that grains are typically homogeneous. Point data for all oxide analyses are given in Appendix B.

Amphibole and biotite phenocrysts were analyzed with a focused beam. Natural mineral standards were used for calibration: CPX1 for Si and Ca; Springwater olivine for Mg and Fe; Orthoclase 1 for K and Al; Tiburon albite for Na; Mn_2O_3 for Mn; TiO_2 for Ti; sodalite for Cl; and fluorophlogopite for F. During analysis, sets of 4–5 replicate analyses of standard Kakanui hornblende and fluorophlogopite were performed to monitor instrument drift. Reported unknown compositions for biotite are averages of 4, to as many as 40, spot analyses per crystal. Relatively high standard deviations indicate that many amphibole phenocrysts are compositionally zoned; thus we report individual spot analyses for this phase. Point data for all biotite analyses are given in Appendix C.

Proportions of mafic minerals within each tephra layer were determined on grain mounts of the 0.125 mm size fraction using an automated stage counting a minimum of 500 points per slide.

Radiocarbon ages were determined on humic-acid extractions from buried soil samples using Accelerator Mass Spectrometry at the University of Georgia Center for Applied Isotope Studies (CAIS) in Athens, Ga. Soil samples were sieved through 125 μm nylon screen, treated with 1N HCl at 80 °C for 1 hr to remove any carbonate material, then washed with deionized water using a centrifuge. Precipitates were treated with 0.1N NaOH to extract humic acids. Alkali solutions were reacted with concentrated HCl to lower their pH to ~2 to precipitate humic acids. Precipitates were collected in centrifuge tubes and rinsed with deionized water to pH of 4–5, then dried at 60 °C. The dry samples were combusted at 900 °C in evacuated sealed quartz ampoules in the presence of CuO. The resulting carbon dioxide was cryogenically purified from the other reaction products and catalytically converted to graphite using the method of Vogel and others (1984). Graphite $^{14}C/^{13}C$ ratios were measured using the CAIS 0.5 MeV accelerator mass spectrometer. Sample ratios were compared to the ratio measured from the Oxalic Acid I (NBS SRM 4990). Sample $^{13}C/^{12}C$ ratios were measured separately using a stable isotope ratio mass spectrometer and expressed as δ13C with respect to international PDB standard carbonate (Keith and Weber, 1964), with an error of less than 0.1 per mil. The quoted uncalibrated dates are given in radiocarbon years before 1950 (yr B.P.), using the ^{14}C half-life of 5,568 years. Errors are quoted as one standard deviation and reflect both statistical and experimental

errors. Dates have been corrected for isotope fractionation. Uncalibrated ages are given throughout the text in order to be compared with other published records of Hayes eruptive products, especially those where uncalibrated age ranges are given in summary and original dates are not known.

The Munsell rock-color chart was used to describe the color of deposits and clasts within deposits. Colors are given for dry samples unless otherwise indicated.

Results

Field Descriptions and Stratigraphy

The Hayes River outcrop lies along the north bank of Hayes River valley, 2 km downstream from the terminus of the Hayes Glacier, and 40 km downvalley from Hayes Volcano (fig. 1). The outcrop is ~600 m long and 30 m high, and consists of a nearly continuous series of bluffs and pinnacles separated by small areas of brush (fig. 2). Three main depositional units make up the Hayes River outcrop, in ascending order: Unit I (the informal Hayes River ignimbrite) is a massive, pumice-rich pyroclastic-flow deposit; Unit II is a flowage sequence and poorly sorted, bouldery diamicton; and Unit III is a tephra-fall sequence consisting primarily of tephra set H (fig. 3). The units generally dip downstream at a greater angle than the riverbed, meaning that the stratigraphically lowest parts of the deposit are exposed at the upstream end of the outcrop.

Unit I: Hayes River Ignimbrite

The basal unit of the Hayes River outcrop is a light gray (N7) to white (N9) pumiceous pyroclastic-flow deposit, the Hayes River ignimbrite (fig. 3). This deposit is 20–30 m thick, and forms the most visually striking part of the Hayes River outcrop (fig. 2). The stratigraphically lowest and largest portion of the Hayes River ignimbrite is a 20-m-thick, lithic-poor (<1 percent) pumiceous, nonwelded pyroclastic-flow deposit (fig. 4*A*). It consists of subangular to subround pumice clasts typically as large as 10 cm (rarely 50 cm) in a fine- to coarse-ash, crystal-rich matrix. The pumice clasts are of two types, (1) dominantly white (N9), friable, biotite-sanidine-plagioclase-quartz rhyolite, with notable foliation caused by alignment of biotite grains, and (2) light gray (N7), finely vesicular rhyolite, less friable than type (1) but with the same mineralogy. Some pumice clasts are texturally banded and are gradational between the two main types. Phenocrysts of feldspar and quartz are as large as 6 mm across. In addition, dense white holocrystalline blocks, also rhyolitic in composition and with the same mineralogy, make up <1 percent of the deposit. The upper 10 m of the Hayes River ignimbrite is lithic-rich, and in some places appears gradational with Unit II.

The total volume of the Hayes River ignimbrite is not known, as it has been recognized only at the Hayes River outcrop. A minimum estimate of 2 km^3 is derived from the total area of the Hayes Glacier drainage upstream (90 km^2) and a minimum thickness at the outcrop of 20 m.

Unit II: Flowage and Bouldery Diamicton Package

Immediately overlying the Hayes River ignimbrite of Unit I is a thick sequence of complex mass-flowage deposits that are variable in thickness along the 600 m wide outcrop (fig. 2). The relation between Units I and II is unclear, as there is some evidence they may be coeval, but for the sake of clarity we describe these flowage deposits as a separate unit.

Immediately above the Hayes River ignimbrite in some places is a 2–4 m-thick sequence of laterally discontinuous, coarse diamicton that includes rounded to angular boulders as much as 2 m in diameter, which are composed of mostly intrusive rocks (granite, granodiorite) and some indurated clasts of volcanic breccia (figs. 4*B*, *C*). No obviously juvenile material was observed in this part of Unit II. The contact between Unit II and the Hayes River ignimbrite below is erosional in some places but graditional in others (figs. 4*B*, *C*). Where the Hayes River ignimbrite is in direct contact with the overlying diamicton, oxidized gas-escape pipes at the contact and upward into the basal boulder diamicton suggest that the ignimbrite may have been hot when the diamicton was emplaced (fig. 4*C*).

The upper several meters of Unit II are a poorly sorted, vaguely bedded, matrix-supported, angular-pebble gravel with an oxidized silt-rich upper 25 cm (fig. 4*D*). The dominant clast type in this upper portion of Unit II is rounded dense rhyodacite with prominent quartz and feldspar phenocrysts in a light gray (N7) matrix.

Unit III: Tephra-Fall Sequence

Tephra fallout, eolian silt deposits, and buried soils make up the uppermost two meters of the Hayes River exposure at site 11HYKLW001 (figs. 1*B*, 2). Tephra deposits generally correlative with tephra set H are exposed ~1 m below the surface and consist of 10 tephra-fall layers distinguished by variations in particle size, bedding, color, or separation by buried soils (figs. 5, 6). The tephra-fall sequence sits on a buried soil with a radiocarbon age of 4,450±30 yr B.P. (table 2). Individual tephra layers range from 1–40 cm thick. On the basis of thickness, grain size, and proximity, eight of the ten tephra-fall deposits were probably erupted from Hayes Volcano (31 km). These tephras were given alphabetic unit names A–H, from oldest to youngest (fig. 5) and were sampled for analysis. Table 3 lists tephra-fall deposit information and table 1 lists basic sample information and type of analysis completed. Tephras F and H are sufficiently thick to be subsampled to test for compositional variation. Six buried soils are evident in this section and all but one were sampled for

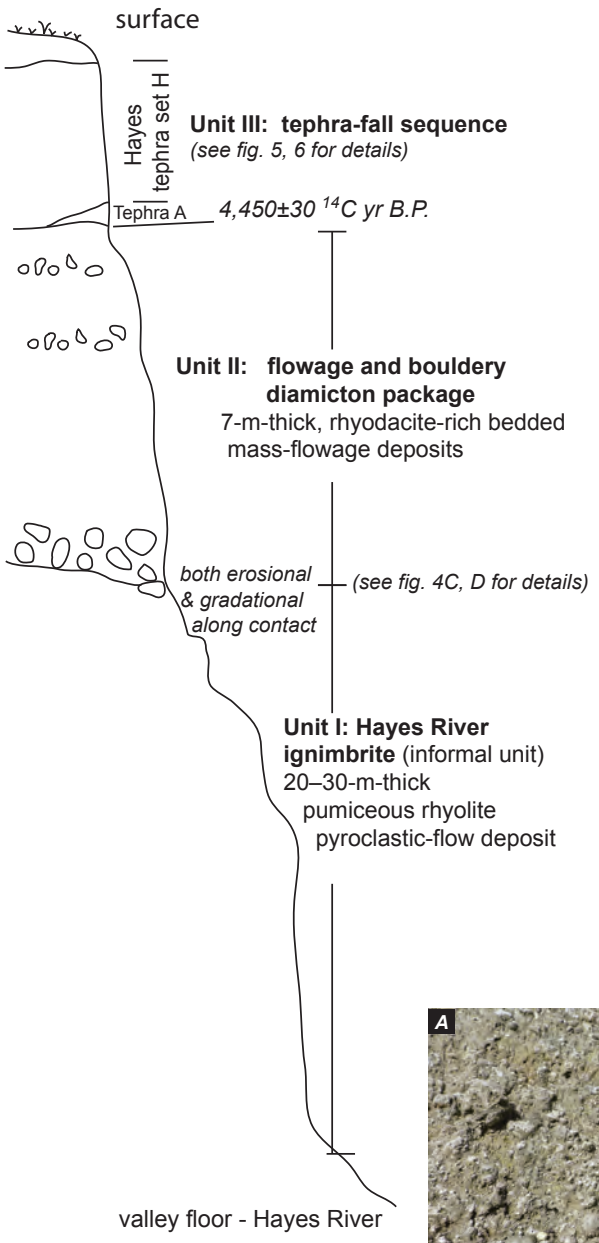

Figure 3. Schematic stratigraphic section of the Hayes River outcrop.

Figure 4. Photographs showing characteristics of Units I and II at the Hayes River outcrop. *A*, Typical matrix-supported, pumice rich, lithic poor exposure of Unit I (informal Hayes River ignimbrite). *B*, Pod of boulder diamicton in lower part of Unit II showing unconformable contact with the underlying Hayes River ignimbrite of Unit I. *C*, Example of gradational contact between Unit I and II. Arrow points to gas-escape pipe in Unit I extending upward into Unit II. *D*, Uppermost part of Unit II showing bedded rhyodacite-bearing volcaniclastic flowage deposit overlain by lower part of Unit III tephra sequence. Arrow pointing to contact between Unit II and III.

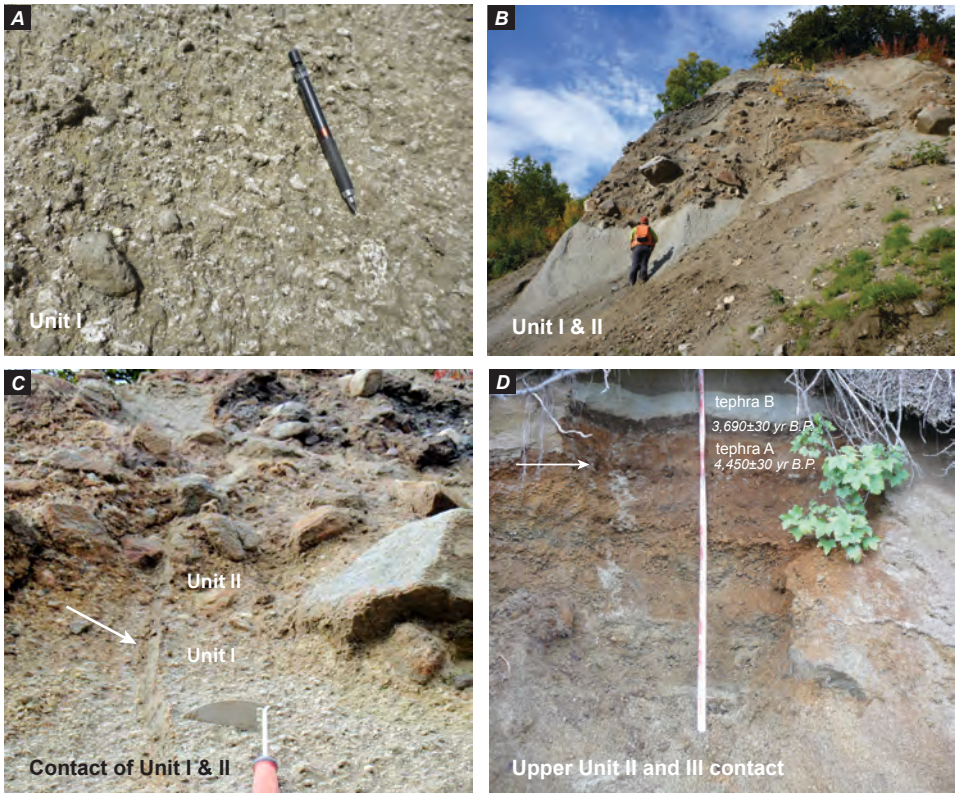

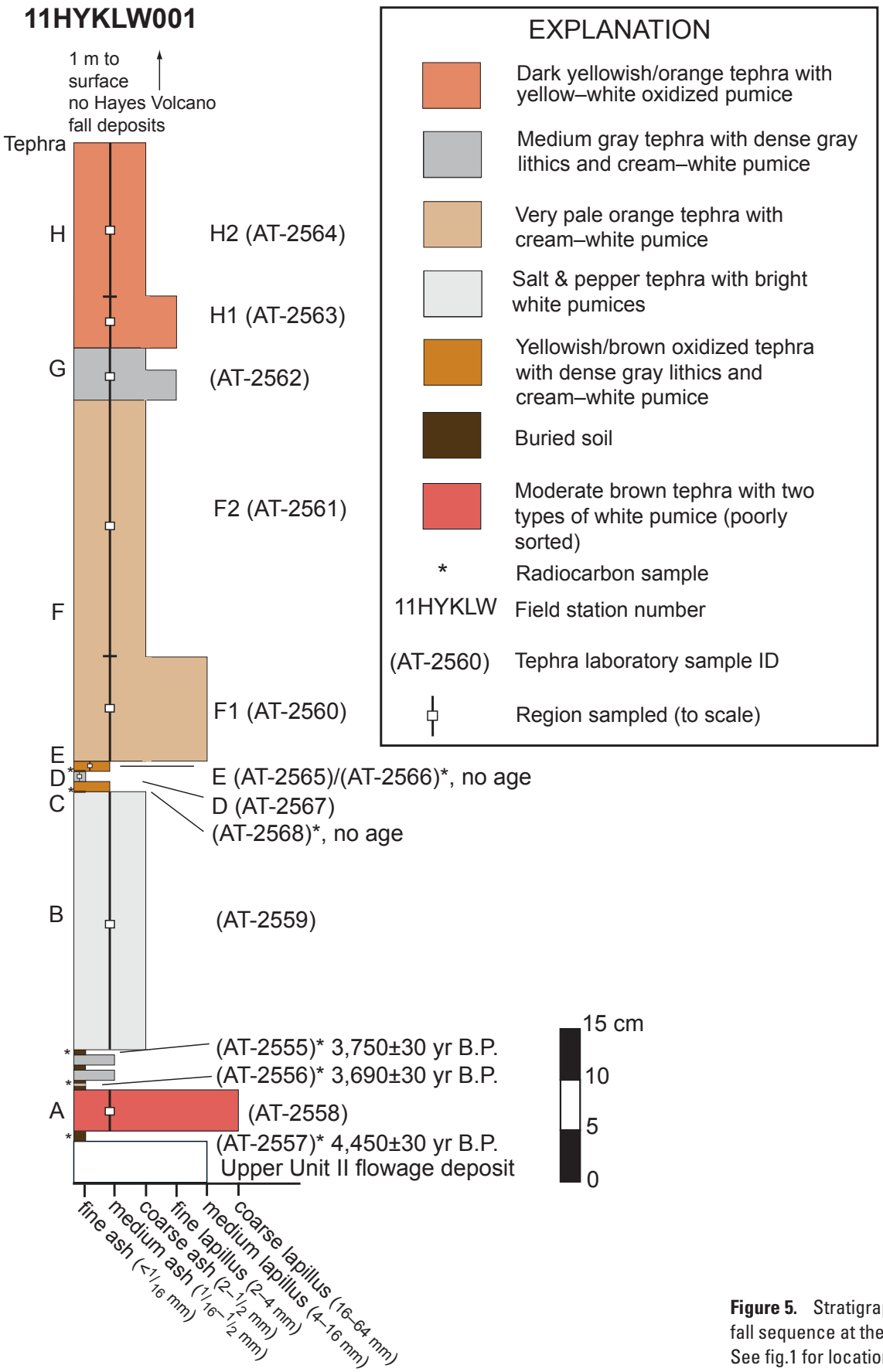

Figure 5. Stratigraphy of Unit III tephra-fall sequence at the Hayes River outcrop. See fig.1 for location.

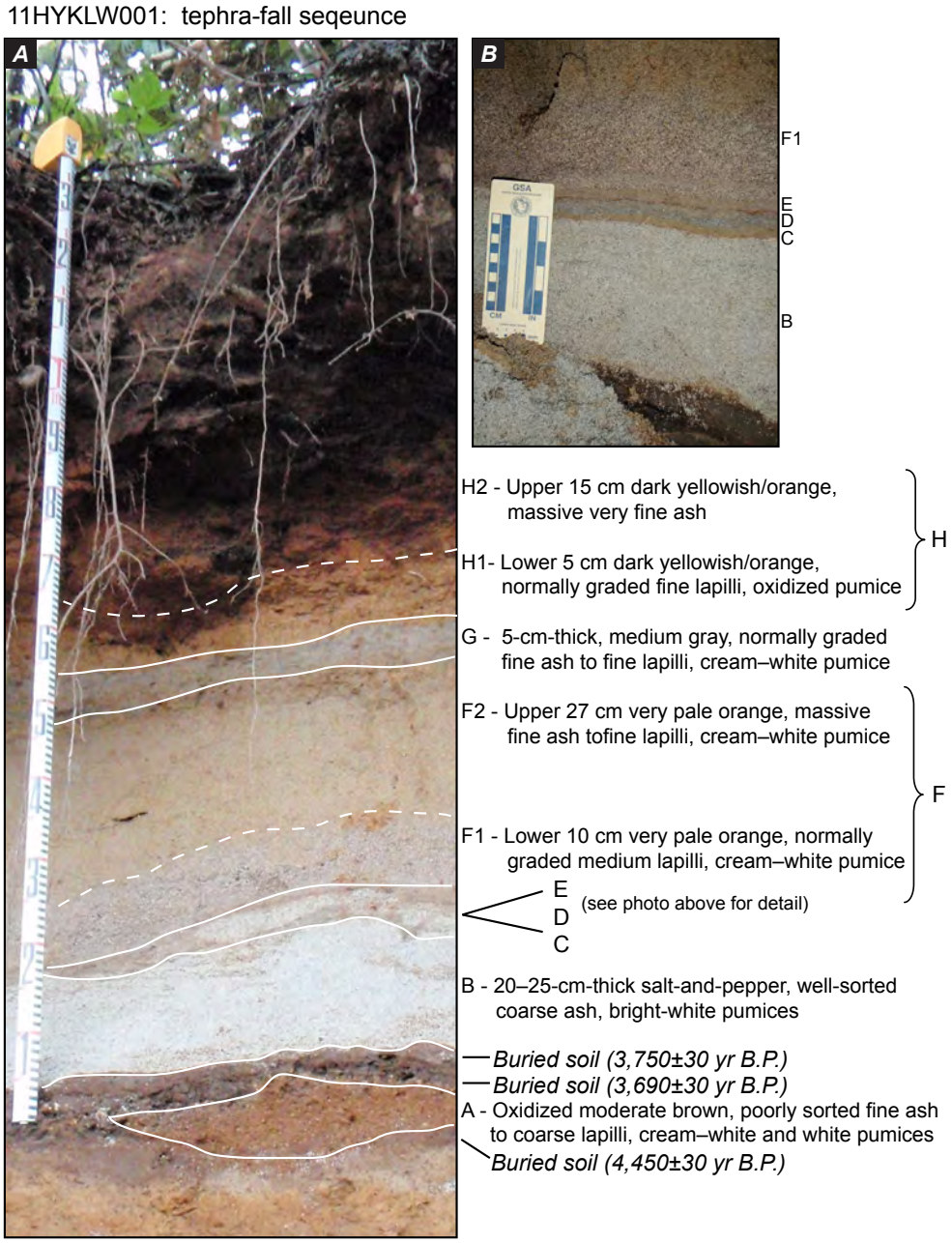

Figure 6. Photographs of Unit III, Hayes River outcrop, showing main tephra layers. *A*, Stratigraphy of Unit III. *B*, Enlargement of photograph showing the lower part of tephra F (F1) through tephra B, with very thin tephra layers C, D, and E visible.

Table 2. Radiocarbon ages from Hayes River outcrop Unit III/tephra-fall sequence.

[ID, identification; B.P. , before present (1950); cal, calibrated; yr, year; ‰, per mil; AMS, accelerator mass spectometry; HA, humic acid extraction from soil material]

Sample ID	AT-#[a]	Lab ID[b]	^{14}C age, yr B.P.[c]	δ^{13}C,‰	Calibrated age, cal yr[d]	Type of analysis
11HYKLW001-4	AT-2557	13291	4,450±30	-26.9	4960-5285 (0.91)	AMS of HA
11HYKLW001-2	AT-2555	13292	3,750±30	-27.3	3987-4162 (0.90)	AMS of HA
11HYKLW001-3	AT-2556	13293	3,690±30	-26.0	3959-4095 (0.90)	AMS of HA

[a] Alaska Tephra Laboratory and Data Center identification number (AT-#)

[b] Lab ID from University of Georgia Center for Applied Isotope Studies, Athens, GA

[c] Uncalibrated ages corrected to δ13C values of -25‰ using listed δ13C values

[d] Ages calibrated to calendar years using the Intcal13.14c calibration curve (Reimer and others, 2013) and CALIB v.7.0 (Stuiver and Reimer, 1993). Calibrated ages shown as 2σ age range (area under probability curve).

Table 3. Descriptions of Unit III tephra-fall deposits from the Hayes River outcrop.

[Colors are from Munsell rock color chart; n/a, not applicable; cm, centimeter]

Sample name	Tephra Lab ID	Unit[a]	Description	Grain size[b]	Thickness, cm	Oxidized	Deposit color, wet	Deposit color, dry	Pumice color, dry	Lithic[c] color, dry	CPX/OPX/ AMP/Bi[d]
11HYKLW001-11	AT-2564	tephra H2	upper 10 cm of 20 cm normally graded fallout	very fine ash to fine lapilli	10	yes	dark yellowish orange (10YR 6/6)	dark yellowish orange (10YR 6/6)	grayish orange oxidized (10YR 7/4)	n/a	0/4/96
11HYKLW001-10	AT-2563	tephra H1	lower 10 cm of 20 cm normally graded fallout	very fine ash to medium lapilli	10	yes	dark yellowish orange (10YR 6/6)	dark yellowish orange (10YR 6/6)	white oxidized (10YR 7/4)	n/a	0/4/96
11HYKLW001-9	AT-2562	tephra G	normal graded fallout	medium ash to fine lapilli	5	no	medium gray (N5)	medium gray (N5)	cream-white (10YR 8/2)	light-medium gray (N6)	0/6/90
11HYKLW001-8	AT-2561	tephra F2	upper 27 cm of 37 cm normally graded fallout	coarse ash to fine lapilli	37–40	yes	very pale orange (10YR 8/2)	very pale orange (10YR 8/2)	cream-white (10YR 8/2-N9)	n/a	0/5/95
11HYKLW001-7	AT-2560	tephra F1	lower 10 cm of 37 cm normally graded fallout	coarse ash to medium lapilli	10	yes	very pale orange (10YR 8/2)	very pale orange (10YR 8/2)	cream-white (10YR 8/2)	n/a	1/5/94
11HYKLW001-13	AT-2565	tephra E	massive	medium to coarse ash	1	no	medium gray (N5)	medium gray (N5)	cream-white (10YR 8/2)	light-medium gray (N6)	0/6/94
11HYKLW001-15	AT-2567	tephra D	massive	coarse ash	1	no	medium gray (N5)	medium gray (N5)	cream-white (10YR 8/2)	light-medium gray (N6)	1/8/92
11HYKLW001-6	AT-2559	tephra B	well-sorted salt & pepper	coarse ash	20–25	no	black and white (N1 and N9)	black and white (N1 and N9)	bright white (N9)	n/a	1/8/92
11HYKLW001-5	AT-2558	tephra A	poorly-sorted fallout	fine ash to coarse lapilli	3–5	yes	moderate brown (5YR 3/4)	moderate brown (10YR 7/4)	bright white (N9) and cream (10YR 8/2)	n/a	1/7/92

[a]Unit refers to alphabetic tephra unit designations shown in fig. 5

[b]Grain-size terms from White and Houghton, 2006. Very fine ash , 1/16–1/8 mm; fine ash, <1/8–1/4 mm; medium ash, 1/2–1/4 mm; coarse ash, 1/2–1 mm; fine lapilli, 2–4 mm; medium lapilli, 4–16 mm; coarse lapilli, 16–64 mm

[c] Lithics refer to dominant, possibly juvenile lithics clasts found in the deposit

[d]Mafic mineral proportions - CPX, clinopyroxene; OPX, orthopyroxene; AMP, amphibole; Bi, biotite

radiocarbon dating. Soil descriptions use basic soil terminology from Birkeland (1999).

Tephra A is the oldest tephra-fall deposit exposed in this section and it sits directly on a weak Aj/Cox buried soil that yielded a radiocarbon age of 4,450±30 ^{14}C yr B.P. An Aj/Cox soil developed on tephra A yielded an age of 3,690±30 ^{14}C yr B.P. (table 2). Tephra A is 3–5 cm thick, oxidized, moderate brown, poorly sorted fine ash–coarse lapilli with both white rhyolite and cream–white dacite pumice (table 3). Between tephras A and B are two thin (mm-scale), fine-grained tephras that were not sampled. Tephra B sits directly on a more mature Aj/Cox buried soil with a radiocarbon age of 3,750±30 ^{14}C yr B.P. (table 2). Tephra B is a 20–25 cm thick, well sorted, non-oxidized, salt and pepper appearing coarse ash with bright white dacite pumice. Tephra C is a 1-cm-thick, oxidized, pale yellowish brown, well-sorted, fine–medium ash with cream–white pumice. The low-carbon Aj/Cox soil beneath tephra C was collected but has not yet been dated. Tephra D is a 1-cm-thick, medium gray, well-sorted coarse ash with cream–white dacite pumice that has a 1-mm-thick iron oxide hard pan at the lower contact with tephra C. Tephra E is identical to tephra C and also consists of a 1-cm-thick, oxidized pale yellowish brown, well-sorted, fine–medium ash with cream–white pumice and a basal iron-oxide hard pan. The low-carbon Aj/Cox soil beneath tephra E was collected but has not yet been dated. Tephra F is a 37–40 cm thick, very pale orange, normally graded, medium lapilli–coarse ash with cream–white dacite pumice. The coarser-grained lower 10 cm of unit F (F1) and the finer-grained upper 27 cm of tephra F (F2) were sampled individually to check for compositional variation. Tephra G is a 5 cm thick, medium gray, normally graded fine lapilli–coarse ash with cream–white dacite pumice. Tephra H is the stratigraphically youngest tephra in the sequence, although its age has not been determined. Tephra H is 20 cm thick, dark yellowish orange, normally graded, and contains fine lapilli–very fine ash with grayish orange oxidized dacite pumice. The coarser grained lower 5 cm of tephra H (H1) and the finer-grained upper 15 cm of tephra H (H2) were sampled individually for compositional variation.

Tephras A, B, F, G, and H contain abundant coarse, vesicular juvenile material and represent the most significant and distinctive fallout deposits of the Hayes River exposure. Tephras B, F, and H are sufficiently thick (≥20 cm) that they are the most likely to represent aerially extensive deposits. One meter of eolian silt (loess) overlies tephra H and is capped by modern vegetation.

Sample Descriptions

Basic information and type of analyses completed for all samples collected from the Hayes River outcrop are given in table 1.

Units I and II: Hayes River Ignimbrite and Flowage/Diamicton Package

Clasts of rhyolite pumice of the Hayes River ignimbrite are generally inflated and glassy and are either bright white or light gray. Using mass balance of whole-rock and mineral compositions in order to calculate modal proportions, they contain approximately 9 percent quartz, 8 percent plagioclase, 7 percent sanidine, and 3 percent biotite in a microlite-free clear glassy matrix (fig. 7*A*). Zircon, monazite, xenotime, apatite, and barite are present in trace amounts. Phenocrysts are as large as 6 mm across and commonly are fractured or fragmented. Dense white blocks have the same phenocryst assemblage and relative abundances as the pumice, but phenocrysts are set within a void-free intergranular groundmass of plagioclase, sanidine, quartz, cordierite, and ilmenite (fig. 7*B*). Because of the similarity in mineralogy and composition to Hayes River ignimbrite pumice, we refer to these clasts as "cognate inclusions". A clast of indurated volcanic breccia from the upper portion of the Hayes River ignimbrite contains glassy fragments with unaltered phenocrysts of plagioclase, quartz, amphibole, biotite, and Fe-Ti oxides (fig. 7*C*).

The majority of clasts in the upper portion of Unit II are relatively dense, light gray, and contain phenocrysts of quartz, plagioclase, apple-green amphibole, and ilmenite in a microlite-rich, biotite-bearing groundmass (fig. 7*D*).

Unit III: Tephra-Fall Sequence

Tephra-fall samples are discussed from oldest (tephra A) to youngest (tephra H), and include descriptions of bulk materials in the size fraction ≥0.125 mm examined with a binocular microscope, as well as loose grain mounts of the 0.125 mm size fraction, and polished, epoxy-impregnated electron microprobe mounts using a petrographic microscope and scanning electron microscope, respectively. The AT- numbers reported after each sample are the U.S. Geological Survey-Alaska Volcano Observatory tephra laboratory reference numbers.

Tephra A (AT-2558) is oxidized, which imparts a moderate brown color to the deposit (fig. 6). Tephra A contains two compositions of pumice, a bright white low-silica rhyolite (72.8 weight percent SiO_2 whole-rock composition; all SiO_2 concentrations reported for analyses recalculated to sum to 100 weight percent volatile-free) with high-silica rhyolite matrix glass (76.5 weight percent SiO_2) and a creamy white dacite with rhyolite matrix glass (70.8 and 72.4 weight percent SiO_2) (tables 4, 5). The sample is dominantly composed of pumice grains (rather than glass shards) and free crystals. Pumices are generally inflated and glassy. Rhyolite lapilli contain feldspar and quartz in a glassy groundmass with biotite microlites and aligned vesicles (fig. 7*E*). Plagioclase and amphibole are the dominant phenocrysts phases in dacite lapilli (fig. 7*F*). Proportions of the two lapilli types are unknown. Rare biotite (<1 percent) is observed in all size

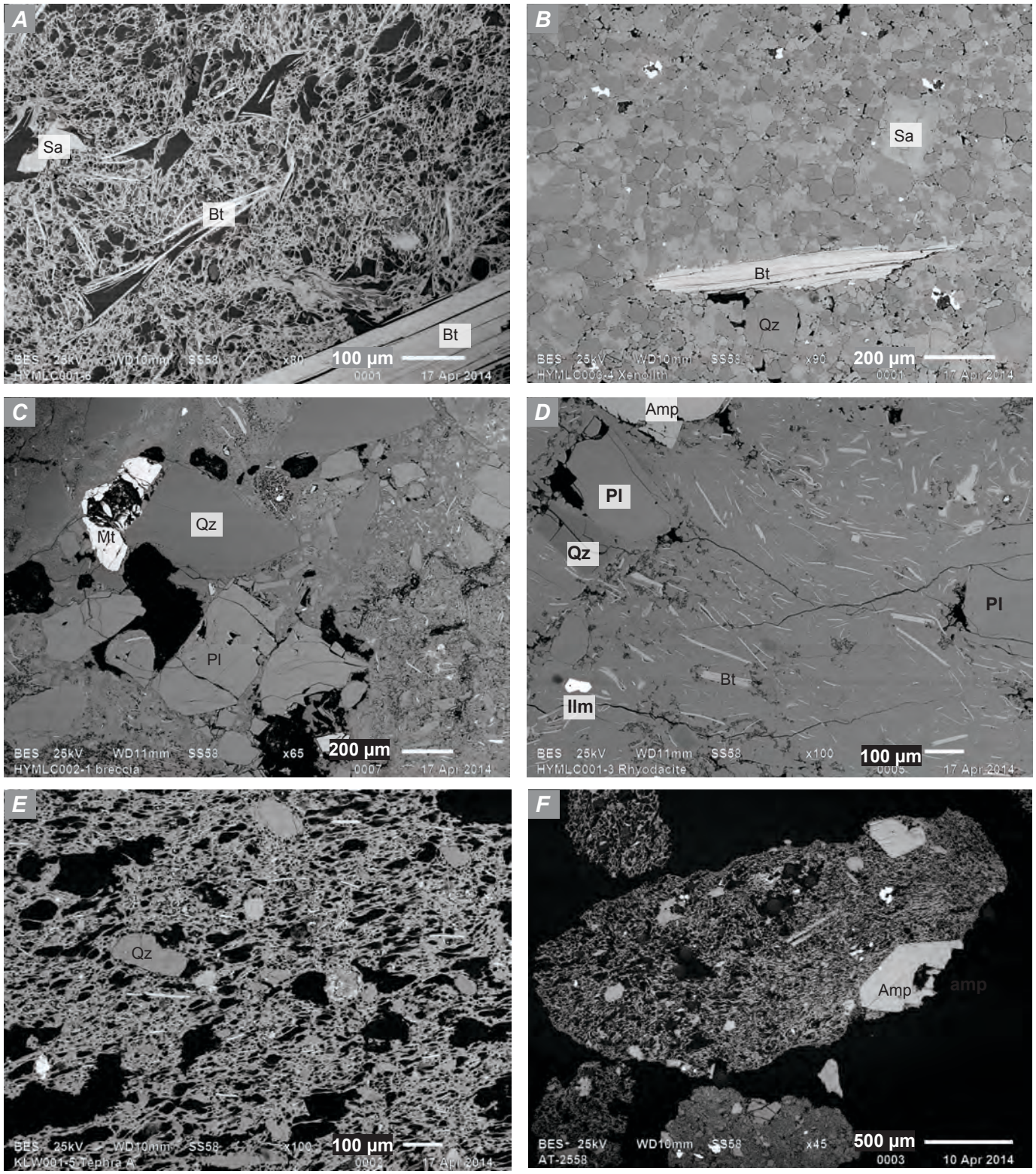

Figure 7. Back-scattered electron micrographs of samples from the Hayes River outcrop, Hayes lava dome, and lahar deposit from site 00CW203. *A*, Rhyolite pumice lump from informal Hayes River ignimbrite. Biotite is present as microlites and phenocrysts. *B*, Dense cognate inclusion from Hayes River ignimbrite. Intergranular groundmass consists of quartz, plagioclase, sanidine, ilmenite and cordierite. *C*, Clast in breccia from upper portion of Hayes River ignimbrite. Breccia contains many of the same minerals as juvenile clasts. *D*, Dense rhyodacite clast from Unit II. *E*, Rhyolite lapillus from tephra A. *F*, Dacite lapillus from tephra A.

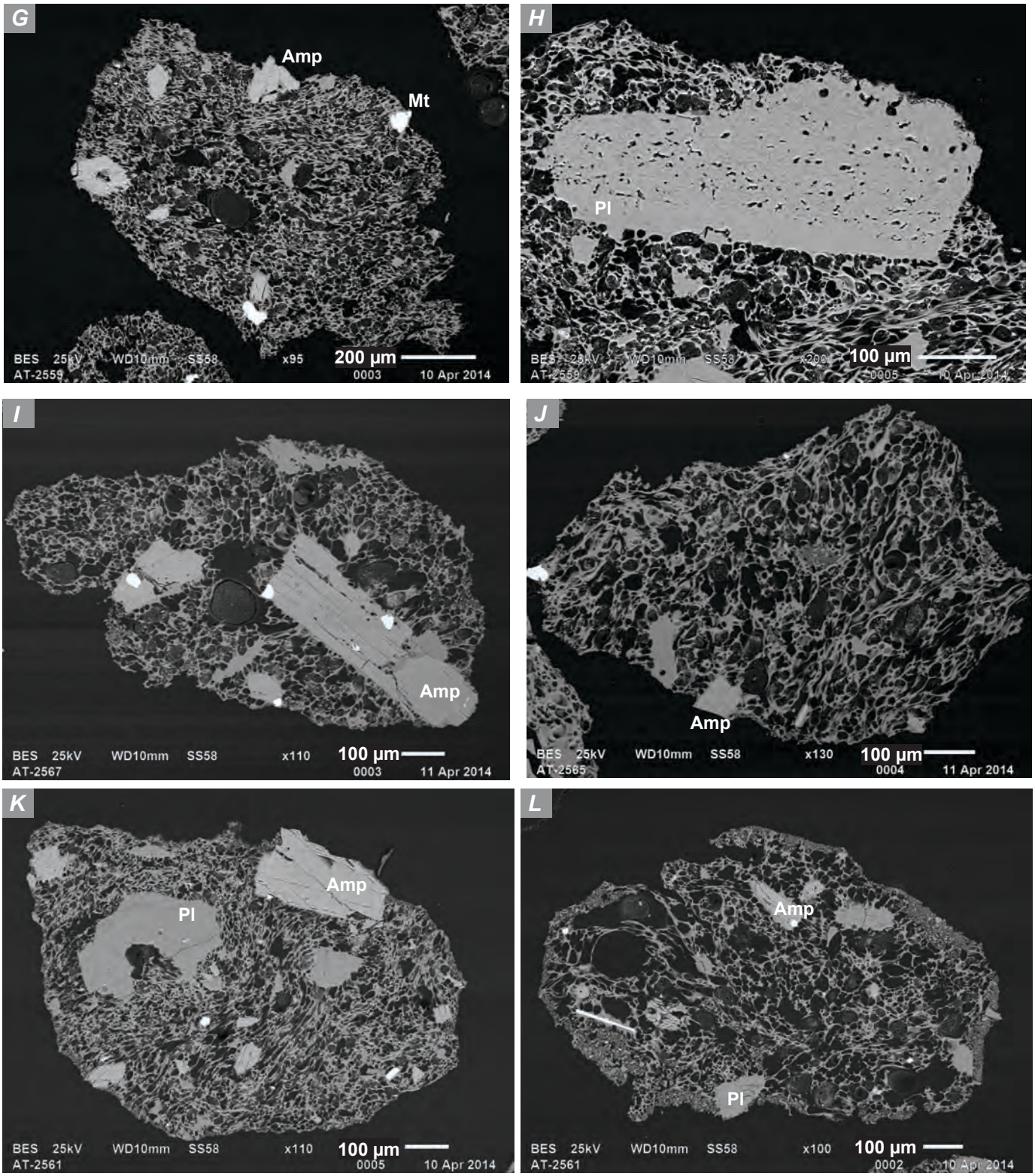

Figure 7.—Continued. *G* and *H*, Lapilli from tephra B. *H* shows example of fritted (sieved) plagioclase, which are common in this tephra. *I*, Pumice lapillus from tephra D. *J*, Pumice lapillus from tephra E. *K* and *L*, Lapilli from upper portion of tephra F showing variations in vesicle textures.

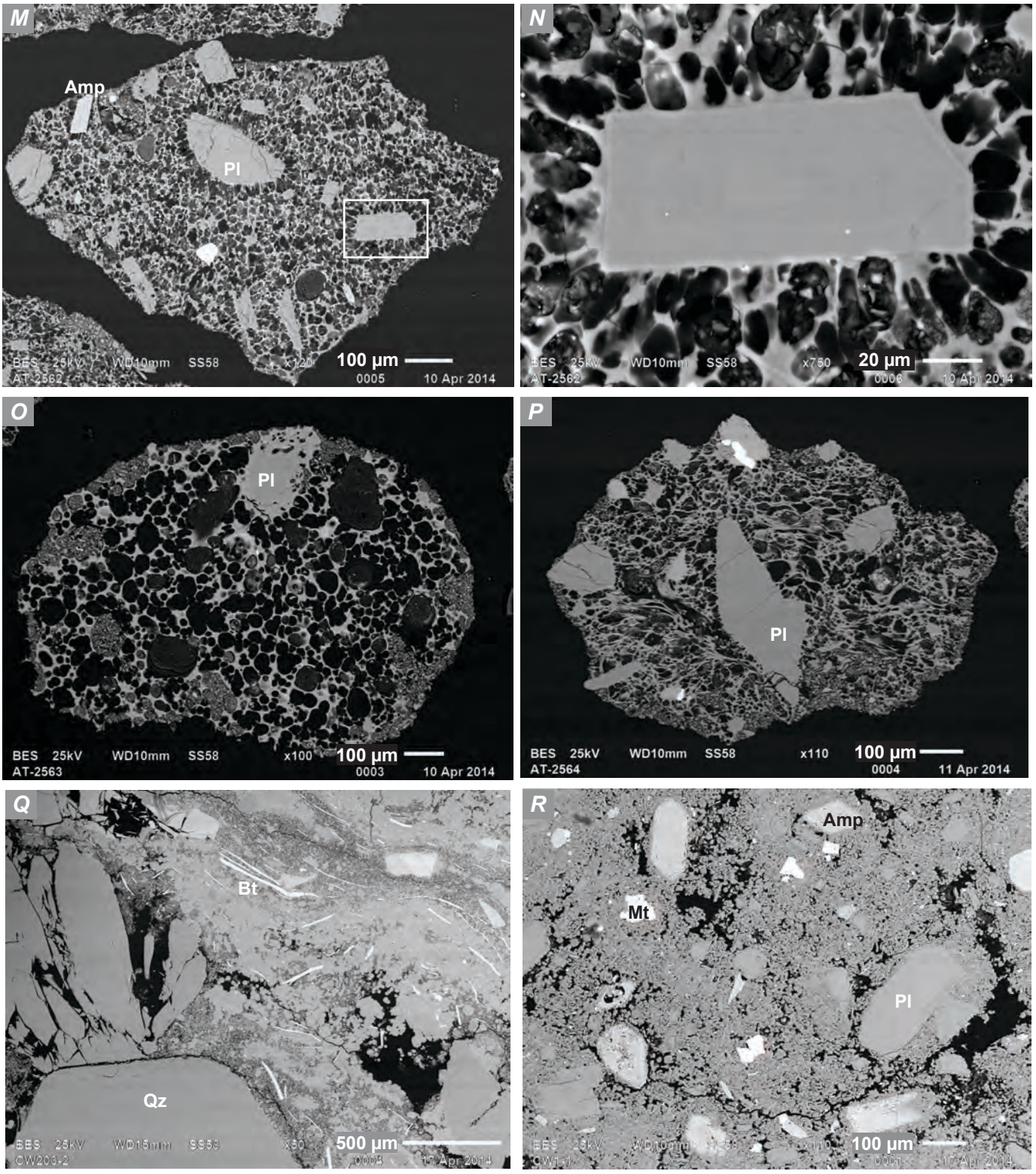

Figure 7.—Continued. *M* and *N*, Lapillus from tephra G. Box on *M* shows location of *N* image showing a euhedral plagioclase crystal. Tephra G groundmass is distinct from the other tephra-fall deposits in being microlite-rich and containing higher-SiO_2 glass. *O* and *P*, Lapilli from tephra H showing range of fluidal groundmass textures. *Q*, Rhyolitic clast from lahar deposit just north of Hayes River outcrop (site 00CW203; fig. 1B). Large, commonly fragmented quartz and sanidine phenocrysts are set in a biotite-bearing groundmass. *R*, Dacite dome material from site 99CW1; fig. 1*B*. Amphibole phenocrysts are rimmed by anhydrous microlite jackets, as is typical of amphibole in effusively erupted intermediate magmas. Mineral abbrevations from Whitney and Evans (2010).

Table 5. Major-element glass compositions from Hayes River outcrop, determined by electron probe microanalyzer at the U.S. Geological Survey in Menlo Park, Calif.

[Reported compositions are weight percent averages of n points, normalized to 100 percent, total gives original sum, 1 σ is standard devation - NOT standard deviation of the mean. Raw point data given in Appendix A. P-, population; n/a, not applicable; orig., original raw total; pum., pumice]

Sample name	AT-#[a]	Unit[b]		SiO_2	TiO_2	Al_2O_3	FeO_T	MnO	MgO	CaO	Na_2On	K_2O	Cln	P_2O_5	Total $_{orig.}$	n
11HYKLW001-11	AT-2564	III: tephra H2	mean	75.36	0.22	13.73	1.61	0.08	0.42	2.06	3.51	2.57	0.40	0.05	97.32	25
			1 σ	*0.61*	*0.04*	*0.33*	*0.18*	*0.04*	*0.04*	*0.18*	*0.29*	*0.13*	*0.06*	*0.03*		
11HYKLW001-10	AT-2563-P1	III: tephra H1	mean	65.24	0.50	16.48	3.90	0.11	2.00	5.04	4.43	1.84	0.21	0.24	99.48	17
			1 σ	*0.41*	*0.06*	*0.21*	*0.16*	*0.04*	*0.05*	*0.19*	*0.18*	*0.06*	*0.03*	*0.04*		
11HYKLW001-10	AT-2563-P2	III: tephra H1	mean	75.07	0.20	13.75	1.59	0.07	0.39	2.05	3.78	2.66	0.39	0.05	96.27	12
			1 σ	*0.56*	*0.04*	*0.25*	*0.12*	*0.03*	*0.02*	*0.14*	*0.24*	*0.11*	*0.07*	*0.04*		
11HYKLW001-9	AT-2562-P1	III: tephra G	mean	77.75	0.27	12.17	1.32	0.09	0.25	1.36	3.43	2.87	0.45	0.05	94.79	26
			1 σ	*0.86*	*0.04*	*0.60*	*0.12*	*0.03*	*0.03*	*0.27*	*0.23*	*0.15*	*0.06*	*0.03*		
11HYKLW001-9	AT-2562-P2	III: tephra G	mean	74.59	0.19	14.44	1.16	0.08	0.20	2.47	3.90	2.48	0.44	0.05	97.19	2
			1 σ	*0.32*	*0.05*	*0.29*	*0.04*	*0.02*	*0.01*	*0.23*	*0.17*	*0.05*	*0.06*	*0.00*		
11HYKLW001-8	AT-2561	III: tephra F2	mean	74.14	0.21	14.49	1.51	0.09	0.47	2.12	3.93	2.66	0.33	0.06	97.24	29
			1 σ	*0.46*	*0.05*	*0.20*	*0.10*	*0.04*	*0.04*	*0.11*	*0.17*	*0.08*	*0.04*	*0.03*		
11HYKLW001-7	AT-2560-P1	III: tephra F1	mean	71.33	0.29	15.70	1.90	0.10	0.59	2.56	4.32	2.68	0.46	0.07	95.11	12
			1 σ	*0.29*	*0.06*	*0.23*	*0.08*	*0.02*	*0.03*	*0.09*	*0.14*	*0.06*	*0.05*	*0.03*		
11HYKLW001-7	AT-2560-P2	III: tephra F1	mean	72.56	0.28	15.11	1.84	0.09	0.56	2.39	4.10	2.58	0.40	0.08	96.79	9
			1 σ	*0.14*	*0.03*	*0.15*	*0.09*	*0.02*	*0.03*	*0.07*	*0.15*	*0.06*	*0.05*	*0.03*		
11HYKLW001-13	AT-2565	III: tephra E	mean	72.69	0.29	14.76	1.87	0.10	0.59	2.36	4.02	2.79	0.44	0.09	97.03	17
			1 σ	*0.62*	*0.05*	*0.18*	*0.07*	*0.03*	*0.06*	*0.12*	*0.55*	*0.18*	*0.05*	*0.04*		
11HYKLW001-15	AT-2567	III: tephra D	mean	73.64	0.21	14.77	1.48	0.08	0.45	2.04	4.35	2.61	0.31	0.07	95.13	15
			1 σ	*0.97*	*0.07*	*0.45*	*0.19*	*0.03*	*0.06*	*0.19*	*0.26*	*0.14*	*0.05*	*0.04*		
11HYKLW001-6	AT-2559	III: tephra B	mean	72.83	0.27	15.09	1.81	0.09	0.57	2.52	4.27	2.18	0.29	0.08	98.38	27
			1 σ	*0.44*	*0.04*	*0.31*	*0.13*	*0.04*	*0.04*	*0.10*	*0.20*	*0.07*	*0.05*	*0.04*		
11HYKLW001-5	AT-2558-P1	III: tephra A	mean	70.84	0.34	15.87	2.18	0.11	0.72	2.97	4.40	2.10	0.34	0.13	97.16	12
			1 σ	*0.24*	*0.05*	*0.17*	*0.13*	*0.05*	*0.04*	*0.07*	*0.19*	*0.06*	*0.04*	*0.03*		
11HYKLW001-5	AT-2558-P2	III: tephra A	mean	76.50	0.05	14.65	0.56	0.20	0.11	0.64	3.47	3.58	0.12	0.13	93.02	10
			1 σ	*0.51*	*0.03*	*0.33*	*0.13*	*0.04*	*0.03*	*0.05*	*0.13*	*0.32*	*0.03*	*0.03*		
11HYKLW001-5	AT-2558-P3	III: tephra A	mean	72.38	0.24	15.38	1.74	0.09	0.53	2.49	4.07	2.65	0.37	0.06	97.03	4
			1 σ	*0.25*	*0.05*	*0.22*	*0.12*	*0.06*	*0.01*	*0.05*	*0.16*	*0.07*	*0.06*	*0.03*		
11HYMLC001-5	n/a	I: HRI, white pum.	mean	75.62	0.02	14.81	0.49	0.19	0.13	0.60	4.09	3.83	0.05	0.16	95.13	20
			1 σ	*0.22*	*0.02*	*0.11*	*0.07*	*0.04*	*0.01*	*0.04*	*0.15*	*0.15*	*0.02*	*0.03*		
11HYMLC003-2	n/a	I: HRI, lt. gray pum.	mean	75.77	0.03	14.77	0.47	0.21	0.13	0.57	3.91	3.95	0.04	0.14	96.11	12
			1 σ	*0.34*	*0.03*	*0.15*	*0.06*	*0.06*	*0.03*	*0.05*	*0.31*	*0.16*	*0.02*	*0.02*		

[a]Alaska Tephra Laboratory and Data Center identification number (AT #)

[b]Unit refers to stratigraphic unit designation shown in fig. 3, 5: Unit I, informal Hayes River gnimbrite (HRI); Unit III, tephra-fall sequence

fractions. Mafic mineral point counts suggest a high amphibole to pyroxene ratio (table 3, fig. 8). In general, mafic minerals as free crystals are rare compared to pumice grains and felsic crystals. Glass in both lapilli types was easy to analyze by electron microprobe owing to the relatively large areas between vesicles.

Tephra B (AT-2559) is a non-oxidized, clean, salt-and-pepper colored tephra that contains bright white dacite pumice with rhyolite matrix glass (72.8 weight percent SiO_2; table 5). Pumices are highly inflated, glassy, and contain phenocrysts of plagioclase, amphibole, and Fe–Ti oxides in clear microlite-free matrix glass (fig. 7*G*). Plagioclase phenocrysts are notably fritted, or "sieved" (fig. 7*H*), more so than in other tephras in the sequence. Although point count data on pumice grains were not collected because of the small grain size, the pumice grains are relatively crystal poor yet the deposit contains abundant glass-coated free crystals. Rare (<1 percent) biotite grains are observed in all size fractions and exhibit both euhedral and irregular forms. Mafic mineral counts suggest a high amphibole to pyroxene ratio (table 3, fig. 8). Because of the highly vesicular glass, locating areas large enough to analyze by microprobe was difficult.

Tephra D (AT-2567) is dominated by dense, light–medium gray, fresh-looking lithic grains and minor cream–white pumice which impart an overall medium gray color to the deposit in wet and dry samples (fig. 6). The lithic grains and pumice contain phenocrysts of plagioclase, amphibole, and Fe–Ti oxides. Lithic grains have grayish microlite-rich matrix glass (not analyzed) while the pumices have clear rhyolite matrix glass (73.6 weight percent SiO_2) (fig. 7*I*). Rare (<1 percent) biotite grains are observed in all size fractions and exhibit euhedral and irregular forms. Mafic mineral counts suggest a high amphibole to pyroxene ratio (table 3, fig. 8).

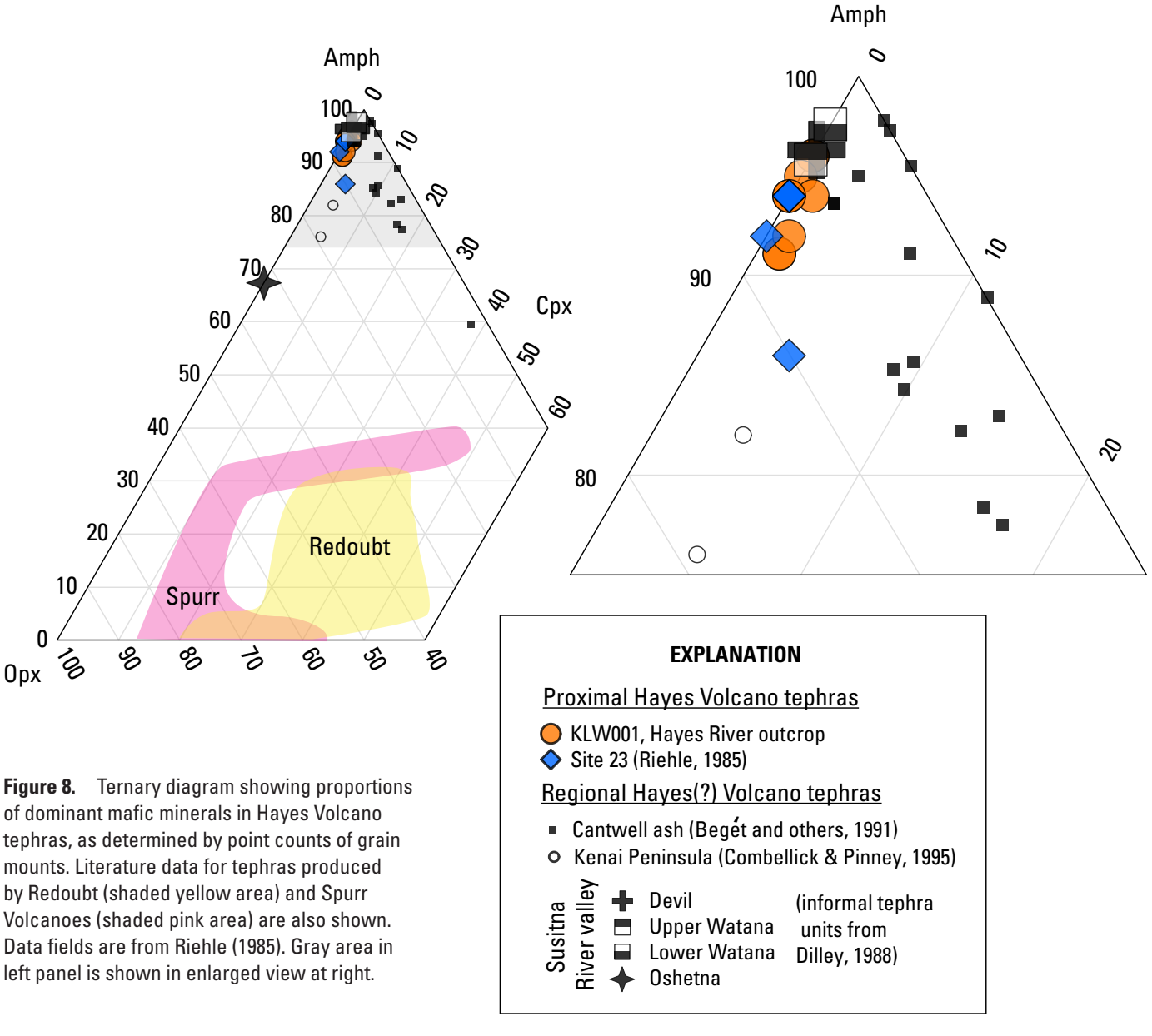

Figure 8. Ternary diagram showing proportions of dominant mafic minerals in Hayes Volcano tephras, as determined by point counts of grain mounts. Literature data for tephras produced by Redoubt (shaded yellow area) and Spurr Volcanoes (shaded pink area) are also shown. Data fields are from Riehle (1985). Gray area in left panel is shown in enlarged view at right.

Tephra E (AT-2565) is dominated by dense, light–medium gray, fresh-looking lithic grains and minor cream–white pumice, which impart an overall pale yellowish brown color to the deposit in both wet and dry samples. The lithic and pumice grains contain phenocrysts of plagioclase, amphibole, and Fe-Ti oxides (fig. 7*J*). The lithic grains have grayish microlite-rich matrix glass (not analyzed) while the pumice grains have clear microlite-rich matrix glass that is rhyolitic in composition (72.7 weight percent SiO_2) (table 5). Biotite is very rare in this sample and only a few grains were observed. Mafic mineral counts suggest a high amphibole to pyroxene ratio (table 3, fig. 8). Despite being microlitic, pumice glass in this sample is fairly easy to analyze with the electron microprobe.

Tephra F is 40-cm thick and was subsampled into two parts, (A) the coarse-grained bottom 10 cm (tephra F1, AT-2560), and (B) the finer-grained upper 30 cm (tephra F2, AT-2561) to assess compositional variation (figs. 5, 6). The overall deposit color is very pale orange. Both samples contain cream–white dacite pumice (WR, 63.8 weight percent SiO_2) with mostly microlite-free rhyolitic matrix glass (71.3–74.1 weight percent SiO_2) (tables 4, 5). Glass composition within the upper unit (tephra F2) appears to have higher silica content (74 percent SiO_2) compared to the lower section (tephra F1, 71–72 weight percent SiO_2). Minor amounts of dense, light–medium gray lithic grains are present but were not analyzed. Pumice >0.250 mm tends to be more oxidized and have a pale yellow brown color while smaller grains (< 0.125 mm) tend to be pure white. Both pumice and lithic clasts contain phenocrysts of plagioclase, amphibole, and Fe–Ti oxides. Rare (<1 percent) biotite grains are observed in all size fractions and exhibit euhedral and irregular forms, including large grains as much as 2 mm in diameter. Mafic mineral counts suggest a high amphibole to pyroxene ratio (table 3, fig. 8). Despite the glass being mostly microlite free, some grains are highly vesicular, making glass analysis difficult (figs. 7*K*, *L*).

Tephra G (AT-2562) is dominated by dense, light–medium gray, fresh-looking lithic grains with minor cream–white pumice, which impart an overall medium gray color to the deposit in wet and dry samples (fig. 6). The matrix glass of the pumice is bimodal high-silica (74.6 and 77.8 weight percent SiO_2) rhyolite (table 5). Both lithic and pumice grains contain phenocrysts of plagioclase, amphibole, and Fe–Ti oxides. The lithic grains have grayish microlite-rich matrix glass, whereas the pumice grains have microlite-free clear glass and microlite-rich grayish glass. Rare (<1 percent) biotite grains are observed in all size fractions and exhibit both euhedral and irregular forms. Mafic mineral counts suggest a high amphibole to pyroxene ratio (table 3, fig. 8). Pumice clasts are generally highly vesicular and the sample is difficult to analyze by electron microprobe because the threads of glass are narrow and microlite-bearing (figs. 7*M*,*N*).

Tephra H is 20-cm thick and was subsampled into 2 parts, (A) the coarse-grained bottom 10 cm (tephra H1, AT-2563), and (B) the finer-grained upper 10 cm (tephra H2, AT-2564) to assess compositional variation (fig. 5). Unit H contains grayish orange oxidized pumice, which imparts a dark yellowish orange oxidized color to the deposit in wet and dry samples (fig. 6). A minor amount of dense, light–medium gray lithic material is present in this sample but was not analyzed. The pumice matrix glass is clear, microlite-rich, and vesicle textures are generally fluidal (fig. 7*O*,*P*). Glass from the lower part of tephra H (H1) is bimodal with nearly subequal populations of dacite and rhyolitic (65 and 75 weight percent SiO_2) while glass from the upper part of tephra H (H2) has an entirely rhyolite composition (75.3 weight percent SiO_2). Rare (<1 percent) biotite grains are observed in all size fractions and exhibit euhedral and irregular forms. Mafic mineral counts suggest a high amphibole to pyroxene ratio (table 3, fig. 8). Despite the glass being microlitic, this sample is fairly easy to analyze on the electron microprobe owing to the relatively large areas between vesicles.

Other Samples

Samples of a lava dome on the Hayes edifice, juvenile clasts from lahar deposits along and near Hayes River, and a tephra-fall near the terminus of Trimble Glacier were collected in 1999 and 2000 (fig.1*B*; table 1). If available, we have included sample descriptions and whole-rock and mineral compositions for these samples.

Two dome samples from field site 99CW1 are very light gray, dense dacite with phenocrysts of plagioclase, oxyhornblende, orthopyroxene, and Fe–Ti oxides in a microlite-rich groundmass (fig. 7*R*). Rare olivine and quartz grains are resorbed, and amphiboles have reaction rims of anhydrous minerals.

A single lapillus from a fall deposit near the terminus of the Trimble Glacier, 00CW201-1, is dacitic and likely correlates broadly to tephra set H (table 1).

Samples 99CW4-1 and 99CW5-2 are from lahar deposits exposed 8 and 18 km, respectively, downstream of the Hayes River outcrop along the Hayes River. Both are cream-colored pumice and dacitic in whole-rock composition.

Sample CW203-2 is a dense rhyolite clast collected from a possible lahar deposit in the drainage just north of the Hayes River outcrop (fig. 1*B*). The sample contains plagioclase, sanidine, quartz, and biotite phenocrysts in a flow-banded groundmass (fig. 7*Q*). Zircon crystals are visible in thin section. Finally, a pumice collected in 1999 from the Hayes River outcrop (sample 99CW3-3) is rhyolitic and likely from the Hayes River ignimbrite (Unit I).

Whole Rock Compositions

Bulk composition by whole rock analysis of juvenile clasts in unconsolidated deposits and lavas is the most common type of analysis used in mapping and correlating proximal volcanic deposits. Bulk composition of tephra-fall deposits, however, change with distance from the volcano

due to density fractionation, so glass and mineral analyses are used instead because they do not change with distance. When working in volcano-proximal settings where coarse-grained juvenile lapilli are commonly found in fallout deposits, whole rock analysis of such clasts are useful for correlation with other volcanic deposits (for example, domes and lahar and pyroclastic-flow deposits) where glass analyses are not common. Lapilli from two Unit III tephra-fall layers (fig. 5, tephras A and F1) were coarse enough for whole-rock analysis. In addition, we analyzed multiple juvenile-appearing clasts from Units I and II, as well as several juvenile clasts from other outcrops collected in 1999 and 2000 (table 1).

The whole-rock compositions of these samples fall into three compositional clusters: dacite, rhyodacite, and rhyolite (fig. 9; table 4). Dacites range from 63.5–64.5 weight percent SiO_2 and include the lava-dome samples, juvenile clasts from lahar deposits along Hayes River downstream from the outcrop discussed herein (fig. 1), and tephra F1 from the Hayes River outcrop. Prior to this report, the only published whole-rock analysis of Hayes eruptive products was of a single pumice lapillus collected on the edifice by Riehle and others (1990). This sample falls within the dacite cluster for the reported major oxides (fig. 9). While the majority of tephra samples attributed to Hayes Volcano do not have whole-rock analyses, it is likely that they fall within the dacite compositional cluster. Preece and others (1992) note an adakitic signature of Hayes-attributed tephra from interior Alaska on the basis of trace-element analysis of glass shards, and trace element data for dacites presented here are consistent with this magma type (McHugh and others, 2012).

Two apparently juvenile clasts from the upper bedded portion of Unit II are rhyodacites with ~70 weight percent SiO_2. The upper part of Unit II appears monolithologic and thus most juvenile clasts in the unit likely are of similar composition.

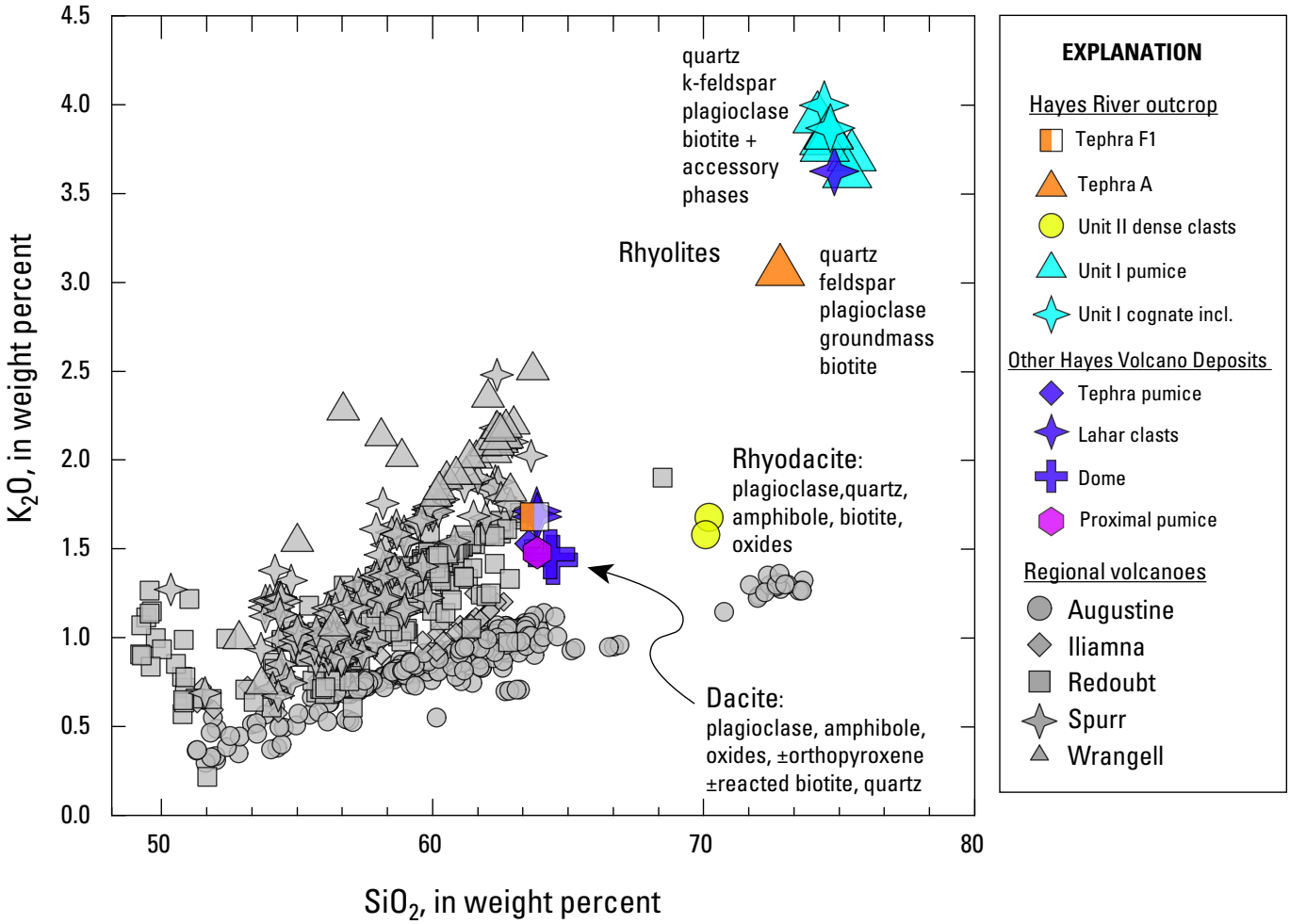

Figure 9. Variation diagram showing whole-rock composition of pumiceous clasts erupted from Hayes Volcano compared to those from nearby volcanoes in south-central Alaska. Note that the informal Hayes River ignimbrite (HRI) pumice, as well as unsourced but possibly related lahar clasts from downstream on the Hayes River, are the most silicic and evolved of all samples shown. Data for non-Hayes Volcano rocks from the Alaska Division of Geological and Geophysical Surveys-Alaska Volcano Observatory (ADGGS) data compilation (Cheryl Cameron, ADGGS, oral commun.). Single, proximal pumice lapillus from Riehle and others (1990). Generalized mineralogy for each sample cluster is also shown.

All other analyzed Hayes Volcano samples, including Hayes River ignimbrite pumice and cognate inclusions, a lahar clast from site 00CW203, and white lapilli from tephra A of the Hayes River outcrop, are rhyolites. They range from 72.8–75.5 weight percent SiO_2, 0.53–0.56 weight percent MgO, and 3.7–3.9 weight percent K_2O (table 4). Whole-rock data from juvenile material in the Hayes River ignimbrite and sample CW203-2 form a tight compositional cluster on all variation diagrams (fig. 9). Tephra A has a slightly lower SiO_2 and K_2O content and also differs in other elements. It is unclear whether this is a result of a true difference in magma composition, or contamination from the analysis of multiple lapilli with perhaps different compositions. The rhyolite eruptive products from Hayes Volcano are distinct from the known eruptive products of other Cook Inlet volcanoes in having higher SiO_2, K_2O, and other incompatible elements (fig. 9; table 1). They are also relatively peraluminous in comparison to other Alaskan Quaternary volcanic rocks, with an alumina saturation index, or molar Al_2O_3/($CaO+K_2O+Na_2O$) values, of 1.1–1.2.

Phase Compositions

Groundmass Glass

Most of the tephra samples contain lapilli with pools of groundmass glass large enough to analyze. Major-element glass compositions range from 65–77 weight percent SiO_2, though excluding the analyses from tephra H, the range is only 70–77 weight percent SiO_2. On most variation diagrams, major-element oxides in the glasses (except tephra G and A) form linear arrays that either decrease (Al_2O_3, FeO, MgO, CaO, Na_2O) or remain flat (K_2O, TiO_2) with increasing SiO_2 (fig. 10). The exception is the tephra G pumice that contains highly evolved groundmass glass (77 weight percent SiO_2) consistent with its high microlite content (fig. 7*M*,*N*). As described above, tephra G has a high lithic content, which paired with its microlitic pumices suggests it may have formed by destruction of a lava dome.

Tephra A has a population of glass that is compositionally distinct from the other (dacitic) tephras and is instead more like the glass from rhyolite pumice of the Hayes River ignimbrite. It has 76 weight percent SiO_2 but falls off the compositional arrays formed by all tephras on oxide variation diagrams, except Na_2O (fig. 10).

Matrix glass from two pumice clasts (one white, one gray) from the Hayes River ignimbrite are indistinguishable within analytical error and have 75.7 weight percent SiO_2, 0.13 weight percent MgO, 14.8 weight percent Al_2O_3, and 3.9 weight percent K_2O (table 5). The Hayes River ignimbrite pumice glasses have significantly higher K_2O and Na_2O, and much lower TiO_2, FeO, MgO, and CaO compared to the overlying dacitic tephras (fig. 10), but are similar in comparison to the most silicic glass population of tephra A.

Fe-Ti Oxides

For dacite tephras, dome rocks, and lahar clasts, the dominant Fe-Ti oxide is titanomagnetite (here called magnetite for simplicity), with ilmenite present in lesser amounts. Magnetite and ilmenite were identified in thin sections of rhyodacite clasts from Unit II, but ilmenite is more abundant and no magnetites were analyzed. Cognate inclusions in the Hayes River ignimbrite contain small ilmenite microlites in the groundmass. Fe-Ti oxides are rare to absent in rhyolite pumice from the Hayes River ignimbrite; of the several thin sections investigated, only two small needle-like opaque crystals were identified (and none analyzed). Individual point data for all oxide analyses are given in Appendix B.

The majority of Fe-Ti oxides that we analyzed are magnetite, and they show distinct variations, especially in minor elements, that distinguish the various tephra deposits of Unit III (table 6; figs. 11, 12). For example, magnetite grains from tephras H1 and H2 form a tight compositional cluster at ~2.6 weight percent Al_2O_3 and ~1.5 weight percent MgO. This suggests that H1 and H2 are components of a deposit from a single eruption of a homogeneous magma (fig. 6). Tephra E also contains homogeneous magnetite grains, with 2.95 weight percent Al_2O_3 and ~1.9 weight percent MgO. Tephras F1 and F2 are relatively homogeneous and overlap with one another, although F1 magnetite has generally lower Al_2O_3. This suggests, like H1 and H2, that tephras F1 and F2 originated from a single eruption. Finally, magnetites from dacitic dome sample 99CW1-1 are also relatively homogeneous, and distinct from nearly all tephra magnetites, indicating that the dome does not correlate directly with any of the tephras at the Hayes River outcrop.

We analyzed fewer magnetite grains from tephras D and G, but they appear to have more diverse magnetite populations (figs. 11 and 12). Tephra G contains magnetite grains that plot squarely with those found in dome rocks but also includes some grains that are more similar to tephra F.

Because we performed oxide analyses on pumice grain mounts and not on mineral separates, the number of ilmenite analyses is small, making it difficult to draw conclusions from these data. Our analyses show, however, a clear distinction between ilmenite compositions of dacitic tephras and ilmenite found within rhyodacitic and rhyolitic samples (fig. 11). Ilmenites from the more evolved rocks have higher FeO (>66 weight percent FeO) and in particular are distinct from the ilmenites in dacite tephras in having much lower MgO (<0.5 weight percent versus >1 weight percent). Ilmenite compositions reported by Riehle and others (1990) are all >1 weight percent MgO, confirming that the tephras at their site 23 are all of the dacitic variety.

We analyzed three touching magnetite-ilmenite pairs in tephra samples. These yielded temperatures of 816–840 °C, and oxygen fugacities of 1.46–1.52 log units above the nickel-nickel oxide buffer (table 6), using the algorithm of Ghiorso and Evans (2008).

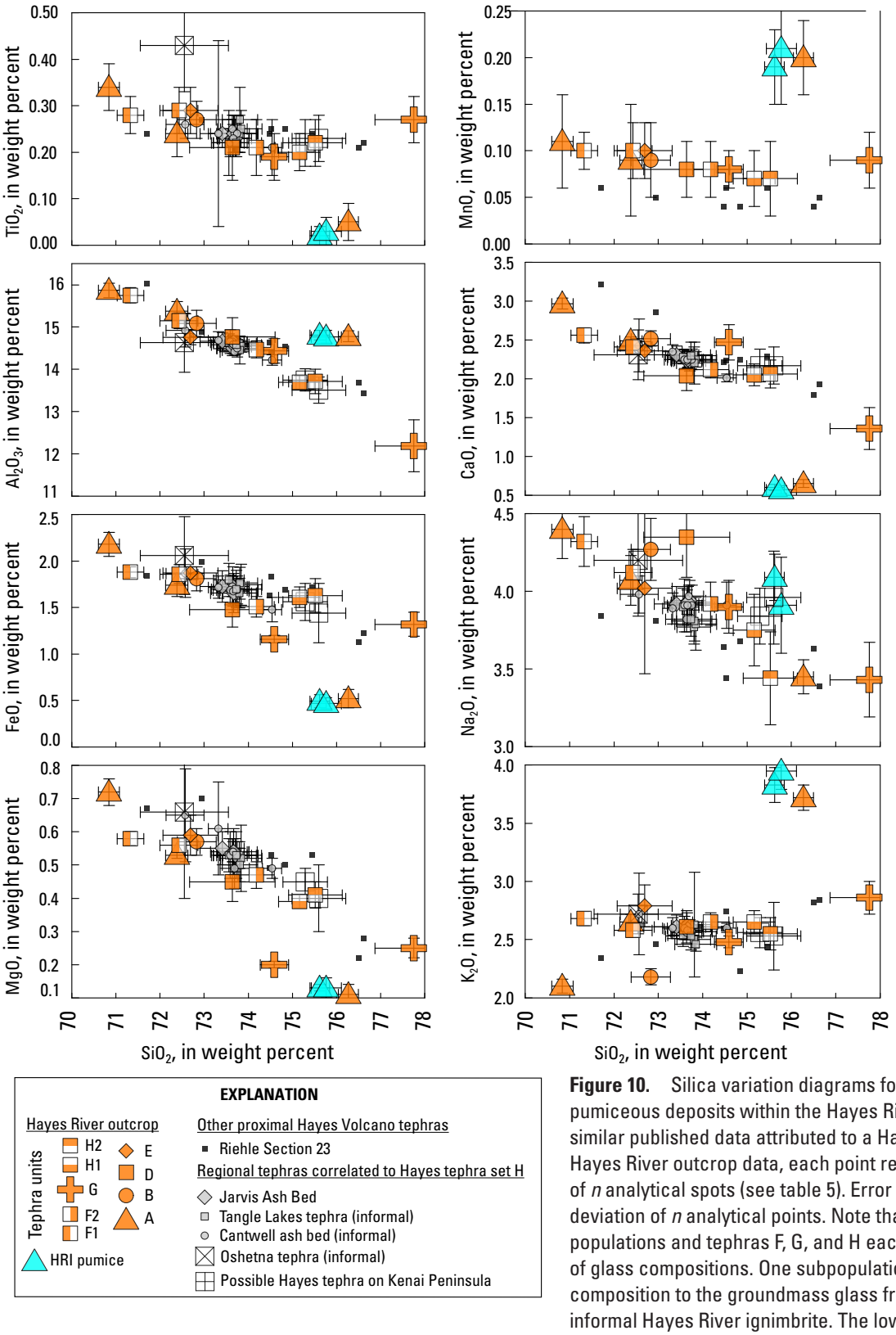

Figure 10. Silica variation diagrams for groundmass glass of pumiceous deposits within the Hayes River outcrop and other similar published data attributed to a Hayes Volcano source. For Hayes River outcrop data, each point represents an average value of *n* analytical spots (see table 5). Error bars represent ±1 standard deviation of *n* analytical points. Note that tephra A has three populations and tephras F, G, and H each contain two populations of glass compositions. One subpopulation from tephra A is similar in composition to the groundmass glass from pumice in the underlying informal Hayes River ignimbrite. The low-silica subpopulation of tephra H (65 weight percent SiO_2) is not shown and plots off axis (table 5). Error bars for Riehle (1994) values removed for clarity as they are generally much larger (see text for discussion). The informal Oshetna tephra composition from Child and others (1998); Hayes Volcano Tephra on Kenai Peninsula correlative with Hayes tephra set H compositions from Combellick and Pinney (1995).

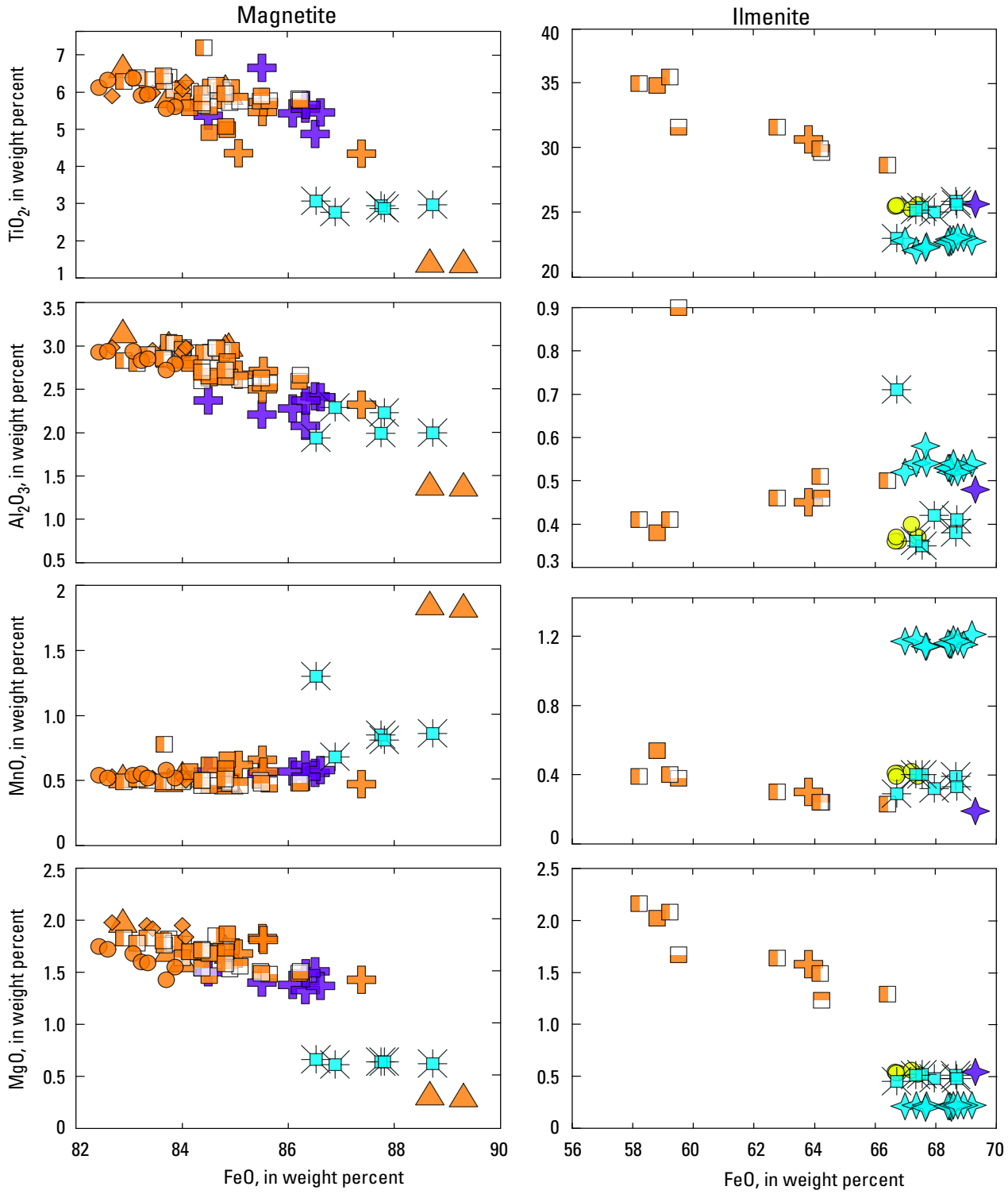

Figure 11. Magnetite and ilmenite compositions for Hayes River outcrop and other Hayes Volcano samples. Each point represents an average of 4–6 analyses on a single crystal. Note that several samples only contain ilmenite; pumice from the informal Hayes River ignimbrite (HRI) is nearly oxide-free and no oxides were analyzed.

Amphibole

Amphibole is the primary mafic phase in all of the rock samples from Hayes Volcano except for the Hayes River ignimbrite rhyolite, the rhyolite pumice of tephra A, and a rhyolitic clast from site 00CW203. All amphiboles in this study are calcic, and are classified as magnesiohornblendes, tschermakites, and magnesiohastingsites, with a few pargasites and edenites, according to the naming scheme of Leake and others (2003). All of the amphiboles are euhedral and lack reaction rims, except for those in dome sample 99CW1-1, which are the only studied amphiboles surrounded by reaction rims of anhydrous minerals.

Many amphibole phenocrysts are compositionally zoned, thus we present individual point analyses as opposed to grain averages (table 7; figs. 13, 14). Dacite lapilli from most tephra units contain both high and low alumina amphiboles that range from 7.2–14.5 weight percent Al_2O_3, with some zoned crystals nearly spanning this range (fig. 13). Five crystals from the dacite dome sample (99CW1-1) are low alumina, whereas tephra B has only high-alumina crystals. The restricted ranges may be a result of the low number of analyzed crystals and should be tested with additional analyses.

Amphibole from rhyodacite clasts within Unit II and a breccia clast from the upper part of the Hayes River ignimbrite are zoned from 9.5–15.5 weight percent Al_2O_3. They mostly do not overlap compositionally with the amphibole of the dacites, and they contain higher FeO and lower MgO at a given Al_2O_3 content (fig. 14). Multiple low-FeO, high-MgO points in fig. 14 are from a single phenocrysts in the rhyodacite.

Biotite

Biotite is present as a stable phenocryst phase in the rhyolite of the Hayes River ignimbrite, the rhyodacite in Unit II, and in the rhyolite lahar clast from site 00CW203. Tephra A contains rhyolitic pumice with small biotite crystals in the groundmass. Rare, reacted biotites are present in some of our dome samples and mounts of the dacitic tephra pumice lapilli. Biotites of different sizes were identified in all tephra-fall deposits mainly as loose grains rather than as phenocrysts within pumices. This may be due to the difficulty in identifying rare phases in very small pumices (<0.250 mm). Because all biotite analyses were done on pumice grain mounts rather than on loose grain mounts, where biotite would have been present in rare (<1 percent) quantities, these loose grain biotites have not been analyzed.

We performed as many as 46 point analyses on some biotite crystals to look for compositional zoning (Appendix C), but all analyzed grains show little internal variation. Biotite compositions fall into two broad clusters. First, biotites from all samples that fall in the "rhyolite" group (Hayes River ignimbrite pumice and cognate inclusions, lahar clast 00CW203-2, and lapilli from tephra A) have lower SiO_2 and

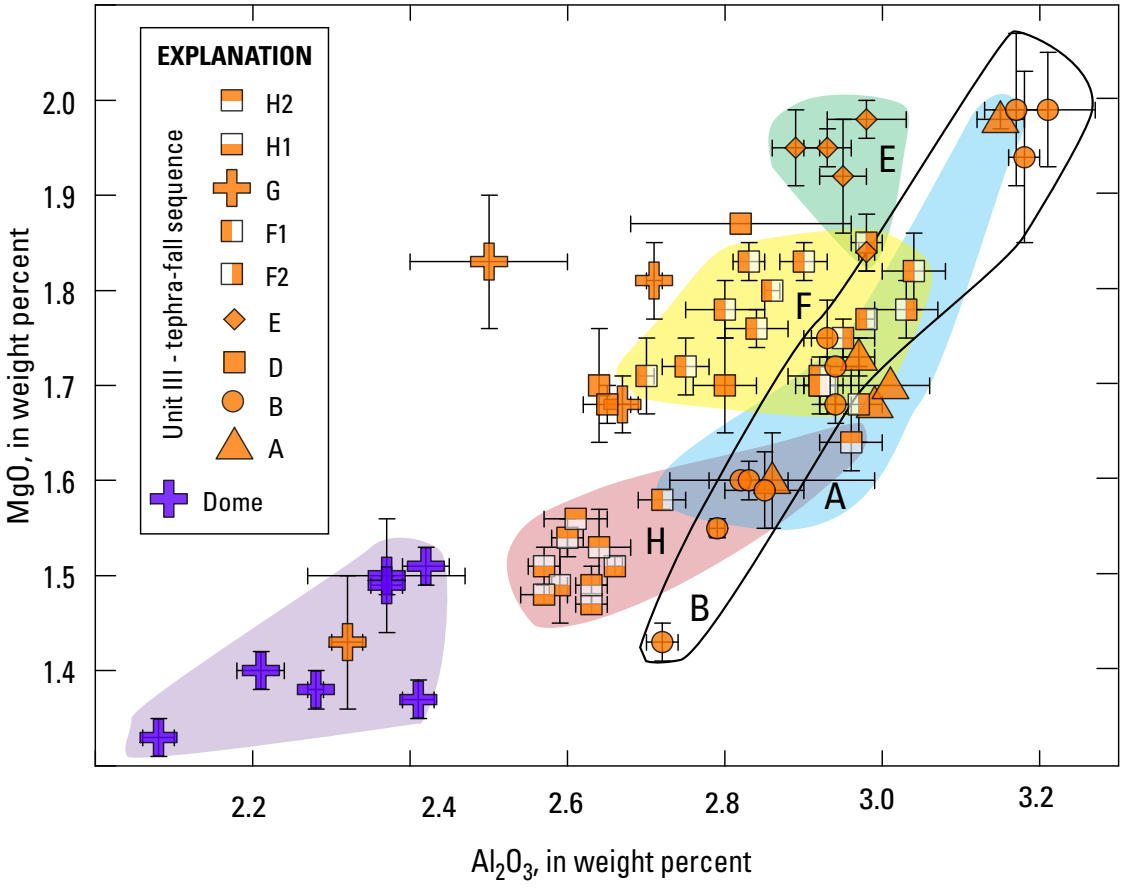

Figure 12. Minor-element variation diagrams for magnetite crystals from dacitic tephras from the Hayes River outcrop and dome sample 99CW1-1 (see fig. 1*B* for location). Colored fields highlight the compositional ranges of magnetites from tephras with at least five analyzed grains. Note tephras H1 and H2, and F1 and F2, have been combined into single fields. Note that two FeO-rich magnetites from tephra A (presumably from rhyolitic lapilli) plot outside of the graph space.

MgO, and higher MnO, FeO, and Al_2O_3 than biotites from dacitic or rhyodacitic samples (Unit II, dome, and tephra samples) (table 8; fig. 15). Within the rhyolite group there are some differences among samples, but the differences are much smaller than between rhyolitic and other groups. In general, the biotites within rhyolite clasts have compositions consistent with other peraluminous rocks as summarized by Abdel-Rahman (1994).

Biotite grains in samples from the dacitic/rhyodacitic groups fall within the calc-alkaline field on the classification diagram of Abdel-Rahman (1994). Note that biotites in true dacites contain reacted grains, whereas the rhyodacite and breccia clast contain euhedral grains.

Significance of Sample Analyses to Eruptive History of Hayes Volcano

Hayes River Exposure

As concluded by Riehle and others (1990) and confirmed by the current study, the tephra deposits that make up tephra set H are dacitic in composition and correlate broadly to the lava domes on the edifice and probably some of the lahar deposits recognized along the Hayes and Skwentna Rivers. Evidently, activity at the volcano from ~3,500–3,800 ^{14}C yr B.P. was dominated by the eruption of dacitic magmas. Confirmation of this hypothesis awaits further field work closer to the volcano and additional radiometric dating.

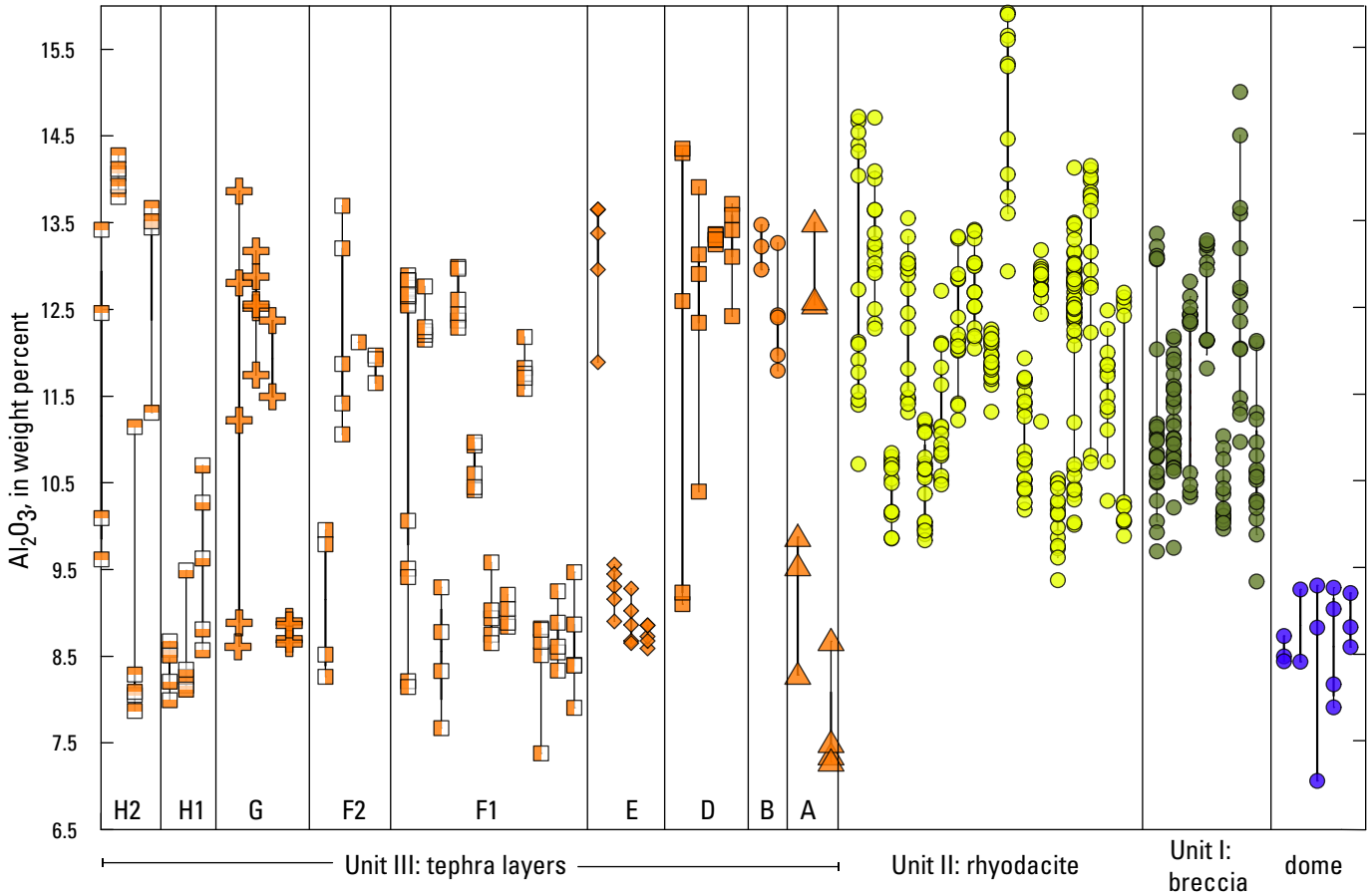

Figure 13. Alumina concentrations of amphibole phenocrysts from Hayes Volcano eruptive products, sorted by deposit. Spot analyses from single crystals are connected by solid black vertical lines. Dacite amphiboles, from the tephra units and dome, form a bimodal distribution with high- and low-alumina populations, whereas rhyodacite and breccia samples form a single population of predominantly zoned crystals. HRI, Hayes River ignimbrite (informal).

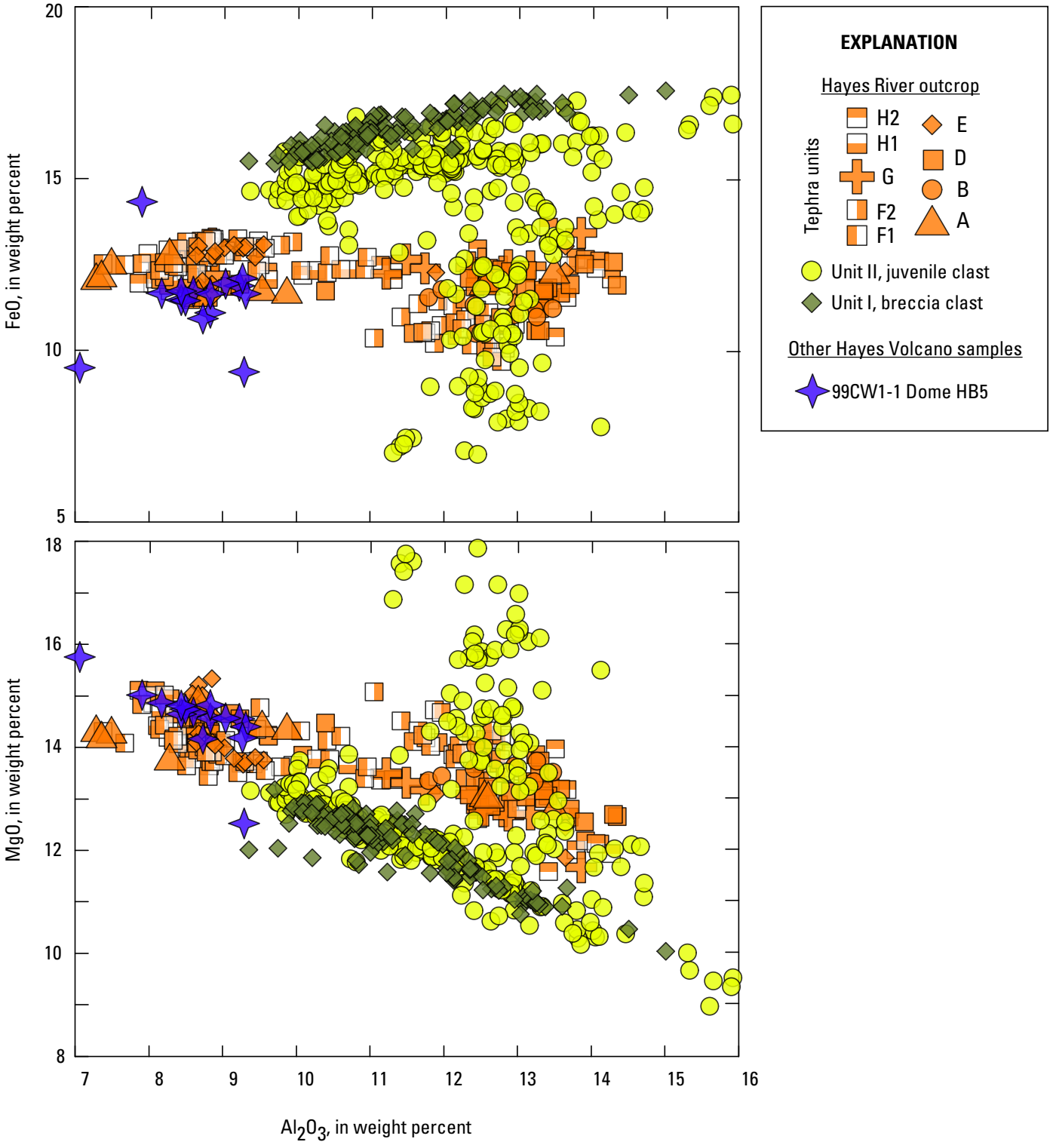

Figure 14. Variation diagrams showing amphibole spot analyses for eruptive products of Hayes Volcano. Each point is a single spot analysis. Low-Fe, high-MgO spots from rhyodacite are almost entirely from two crystals. With the exception of these two crystals, note separate trends for dacite (in other words, tephra and dome) amphiboles versus amphibole from the rhyodacite and ignimbrite breccia clast. HRI, Hayes River ignimbrite (informal).

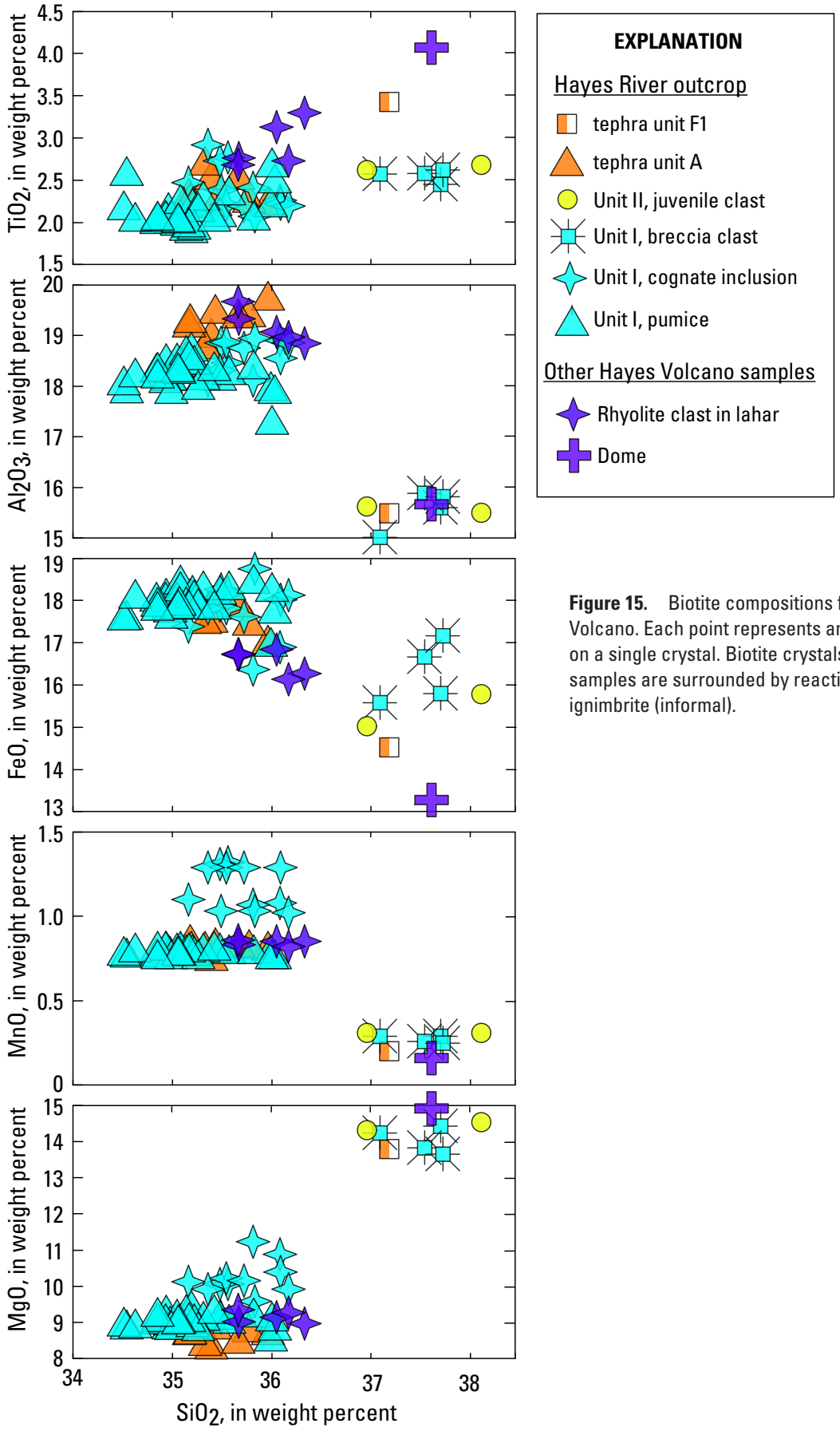

Figure 15. Biotite compositions for eruptive products of Hayes Volcano. Each point represents an average of multiple analyses on a single crystal. Biotite crystals in tephra F1 and dome samples are surrounded by reaction rims. HRI, Hayes River ignimbrite (informal).

Based on mineral assemblages and glass chemistry, all regional tephras thus far attributed to Hayes Volcano generally fall within the dacitic compositional cluster except tephras G and A which my not be regionally extensive (fig. 10). The high proportion of amphibole to pyroxene, and the presence of trace biotite (as we note here, commonly with reaction rims), provides strong evidence for correlation to this general time period of eruptive activity at Hayes Volcano. Distinguishing among tephra set H and other Hayes Volcano tephras is of key interest so that these layers can be used as high-resolution time-stratigraphic markers in other areas of Alaska. The tephra deposits at the Hayes River outcrop represent another reference section for tephra set H and yield promising results for distinguishing among tephra layers. Although major-element glass geochemistry and proportions of mafic minerals alone do not conclusively distinguish among layers of the Hayes tephra set H, the deposits are distinctive in the field in terms of color, particle size, degree of oxidation, and thickness. Thus, photographs (fig. 6) and detailed stratigraphy (fig. 5) should aid in discriminating layers in distal locations (fig. 16). Tephras B, F, G, and H are the most significant and distinctive deposits, and thus are most likely to correlate with distal tephras. Our glass data generally have low standard deviations and higher number of analyses compared to Riehle's (1985) section 23, the only published reference section to date. Fe-Ti oxide geochemistry shows distinct variations between tephras, especially in minor elements (figs. 11, 12). This may prove useful in identifying individual beds within tephra set H in distal settings throughout southern Alaska. Figure 16 summarizes the distinctive features of individual tephra layers at the Hayes River exposure to aid in correlating to other tephras identified in this region.

New results presented here show that Hayes Volcano also has produced rhyodacite and rhyolite magmas farther back in its eruptive history. Tephra A respresents an eruption of rhyolitic and dacitic magma as recent as 4,450±30 ^{14}C yr B.P. The rhyolite component of tephra A is compositionally and mineralogically distinct from the younger dacite tephras. It should be possible to recognize and correlate distal equivalents to tephra A by the absence of amphibole and pyroxene, and an abundance of small biotite grains and quartz in the rhyolite fraction of the deposit. Tephra A magnetites have unusually low MgO and Al_2O_3 and high MnO, which may also be useful for recognizing distal equivalents. Tephra H has a distinct subpopulation of low silica glass composition (65 weight percent SiO_2) not observed in another tephra layer of the tephra set H (table 5).

Older deposits at the Hayes River outcrop include a sequence of flowage and bouldery diamicton deposits (Unit II). The uppermost part of the Unit II flowage deposits is composed dominantly of rhyodacite, and may represent a primary or nearly primary eruptive sequence. No compositionally equivalent tephra deposits correlative with Unit II rhyodacites have yet been identified.

The oldest unit in the Hayes River outcrop is the pumiceous Hayes River ignimbrite (Unit I), which is rhyolitic in composition with a phenocryst assemblage of quartz, sanidine, plagioclase, and biotite that is distinctive among known Quaternary volcanic products of Hayes and other Alaskan volcanoes. Intriguingly, a dense glassy rhyolite clast of nearly identical composition was collected at a nearby outcrop in 2000, but more field work is needed to determine its relation, if any, to the Hayes River ignimbrite. In some places along the Hayes River outcrop, the gradational contact between Units I and II indicates that these units may have been emplaced very closely in time or be a part of the same eruptive sequence.

We have no direct evidence for the eruption age of the Hayes River ignimbrite, however, it must be older than the 4,450±30 ^{14}C yr B.P. soil beneath Unit III. The limited extent of Hayes River ignimbrite deposits may be the result of erosion by glacial ice. Given the thickness, particle size, and composition of the Hayes River ignimbrite, it likely records a substantial eruption of Hayes Volcano, and we would expect to find correlative tephra deposits in many areas of south-central Alaska if the ignimbrite were emplaced during a Holocene eruption. Radiometric dating of sanidine, zircon, and monazite from the Hayes River ignimbrite's rhyolite pumice indicate crystallization ages of ~40–30 ka (Calvert, Coombs, and Vazquez, USGS, unpub. data, 2014), thus representing a maximum possible age. Preservation of pre-Holocene pyroclastic deposits in south-central Alaska is extremely limited, presumably due to emplacement on ice or erosion by glacial ice. Tephra records at Cook Inlet volcanoes rarely are older than Holocene (Fierstein, 2007; Schiff and others, 2008). A few deposits that appear to have survived glacial erosion have been documented as limited-exposure outcrops similar to the Hayes River ignimbrite. For example, ~23 kyr B.P. and 12–16 kyr B.P. pyroclastic-flow deposits from Katmai (Fierstein, 2007; Hildreth and Fierstein, 2000; Hildreth and Fierstein, 2012), and tephra falls as old as 40 ka from Augustine (Waitt and Begét, 2009).

Correlation to Previously Described Hayes Volcano Deposits

Tephras B, F, G, and H of Unit III, as well as the underlying Units I and II, are the most significant and distinctive deposits of the Hayes River outcrop and are the most likely to represent widespread deposits in south-central Alaska. Tephra A contains coarse silicic pumice, but its poorly sorted, discontinuous, and thin-bedded preservation in this setting suggests that more work is needed to understand its significance. All other Holocene tephra deposits at the Hayes River outcrop are either thin, or contain an abundance of dense dome-like fragments and lesser amounts of vesicular pumice, and thus may not be the products of voluminous, aerially extensive tephra plumes.

In an attempt to summarize previously published information on tephra set H and other Hayes Volcano-sourced tephras, table 9 includes glass geochemical data from Riehle

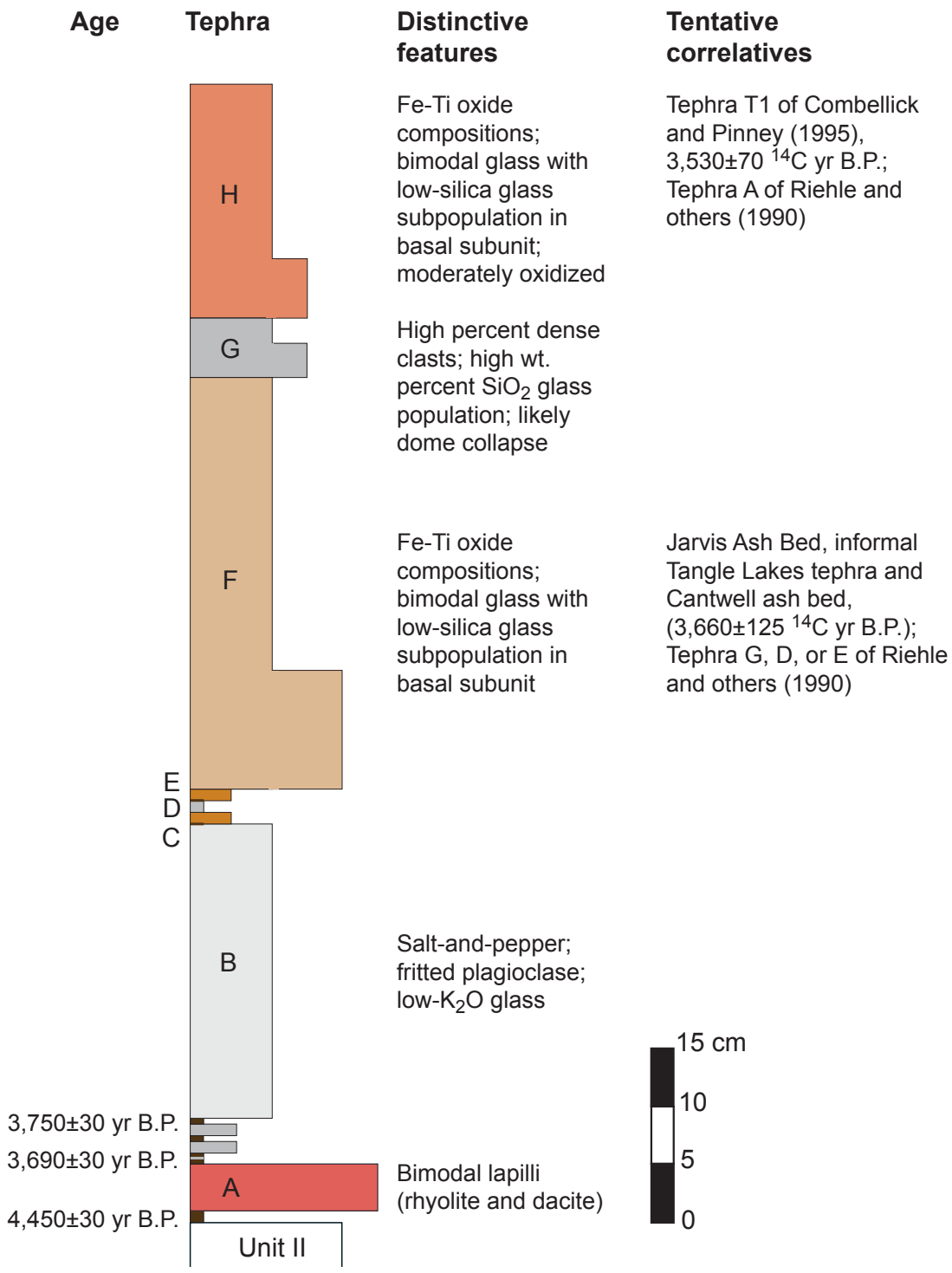

Figure 16. Overview of distinctive features, of and possible correlatives to, the Hayes River outcrop tephra-fall deposits of Unit III.

(1985), Begét and others (1991), Combelick and Pinney (1995), Child and others (1998), and J. Romick (written commun., 1984). Figure 10 shows major-element discriminant plots of these data compared to data from the Hayes River outcrop described in this report. Below we discuss the deposits and present some possible correlations with the Hayes River outcrop. To avoid confusion, we note that reference tephras from Riehle (1985), like ours, have letter names (A–G) but in no way correspond to our letter-named tephras (A–H), as our units were lettered from oldest to youngest and his from youngest to oldest.

Section 23 of Riehle (1985)

Since 1985, the only published reference section for Holocene-age tephra deposits from Hayes Volcano, to which all distal correlatives are compared, is a site in Hayes River Pass (~61.73°N, 151.91°W; fig. 1*B*, site 23), 55 km northeast of Hayes Volcano. The tephrostratigraphy of site 23 in Riehle (1985) is generally similar to that of Unit III at the Hayes River outcrop (fig. 5), except that our tephra A is not recognized at the Hayes River Pass site. Riehle (1985) reports an age range for tephra set H as 3,500–3,800 ^{14}C yr B.P. and describes 7 or 8 individual tephras in the set. Our results are broadly consistent with Riehle's, but more work is needed to better define the spatial and temporal relations of the tephra set, to determine how many discrete eruptions occurred, and to establish the transport directions of the components of the tephra set.

Riehle and others (1990) and Riehle (1994) discuss the compositional variation of individual tephra layers from the Hayes River Pass site, and remark that the major-element glass geochemistry, determined by electron microprobe analysis, is similar among all components of tephra set H. This finding makes geochemical differentiation of the tephras within the set impractical on the basis of glass data alone. We note a similar difficulty in correlating individual tephras from the Hayes River outcrop with the tephras present at site 23.

Riehle (1994) presented glass data for seven tephra-fall layers, 23-A through 23-G from reference section 23 (table 9), that were analyzed by a "9-channel" electron microprobe (3 wavelength-dispersive x-ray spectrometers and 6 fixed monochrometers). Analyses of these layers were first conducted by "3-channel" probe (3 wavelength-dispersive x-ray spectrometers) and presented in Riehle (1985) and Riehle and others (1990). Riehle (1994) reports averages of 2–10 glass shards from crushed lapilli for each layer; it is not clear if crushed shards represent one or multiple lapilli per layer. Riehle (1994) found two distinct glass populations in layers E, E1, and E2, and notes that within-sample major oxide variation is as much or greater than it is among the entire suite of samples representing tephra set H. He concludes that, "such overlap precludes unambiguous correlation of distal samples with a specific reference sample" (p. 285; Riehle, 1994).

Riehle and others (1990) also performed Fe-Ti oxide analyses by EPMA on grain mounts of tephras from their reference site 23, and noted little compositional variation among magnetites, but distinctive ilmenite compositions among the seven units of their section. In particular, site 23 tephras contained both high- and low-FeO ilmenites (56–70 weight percent) in different proportions. Our survey of oxide compositions yielded only nine ilmenite grains from the tephra deposits of Unit III. The limited number suggests a similar bimodality to that documented by Riehle and others (1990). Our results and those of Riehle and others (1990) show that both magnetite and ilmenite are potentially useful correlation tools for Hayes Volcano tephras.

Jarvis, Tangle Lakes, and Cantwell Tephra Deposits

Begét and others (1991) show that regional tephras found in interior Alaska, formally known as Jarvis Ash Bed of Pewe (1975), and informally Tangle Lakes tephra of Begét and others (1991), and Cantwell ash bed of Bowers (1979), are all compositionally identical within error margins and thus represent a single eruption, which they dated at 3,660±125 ^{14}C yr B.P. The mineralogy and glass composition of these tephras indicate that they were erupted from Hayes Volcano (table 9; figs. 8, 10). Begét and others (1991) also conclude that the Jarvis, Tangle Lakes, and Cantwell tephras are similar to units C, D, and E of Riehle and others (1990) at site 23. Riehle (1994) later concluded that the glass chemistry of the Jarvis Ash Bed and unit G at site 23 had the best match and suggested that they were the same tephra. Both studies indicated that multiple glass populations within single tephra horizons can make correlations based on average compositions misleading.

On the basis of major-element glass compositions (fig. 10), we find that the Jarvis Ash Bed correlates most closely with our tephra F, which is the thickest tephra at the Hayes River outcrop (40 cm), and the only tephra that contains medium (4–16 mm) lapilli (fig. 16). This may be consistent with the conclusions of Riehle and others (1990), who indicated that tephra G at site 23 was deposited from a northward-directed ash cloud that would have travelled over interior Alaska.

Southeastern Lobe of Hayes Tephra Set H

Combellick and Pinney (1995) describe a 3-cm-thick tephra on the Kenai Peninsula dated at 3,530±70 ^{14}C yr B.P. They conclude, on the basis of major-element glass chemistry and minerology, that it correlates with unit A of Riehle (1985), the uppermost tephra at his site 23 (table 9, figs. 8, 10). The glass composition of this tephra is most similar to our tephra H, which is also the uppermost tephra at the Hayes River outcrop (fig. 10 and 16).

Oshetna Tephra

The Oshetna tephra, informally named by Child and other (1998) for the stream valley in which it was first identified during cultural resource investigations conducted from 1979–85, is

widespread in the Susitna River valley in south-central Alaska (fig. 1*A*; J.E. Dixon and others, written commun(s)., 1985). The Oshetna tephra is 3–5 cm thick in this region, and is attributed to Hayes Volcano based on similarities in mineralogy and major-element glass composition to Hayes Volcano tephras. The Oshetna tephra was erupted 5,960–5,790 ^{14}C yr B.P. (Child and others, 1998), which makes it older than tephra set H at the Hayes River outcrop. Numerous additional radiocarbon analyses from J.E. Dixon and others (written commun(s)., 1985) corroborate this age. Glass analyses for pumice from the Hayes River ignimbrite do not match glass data for the Oshetna tephra, which have lower SiO_2 and K_2O, and higher CaO, MgO, and TiO_2 than Hayes River ignimbrite glass (fig. 10). Similar amounts of amphibole and biotite in the Oshetna tephra and the rhyodacite clasts from Unit II at the Hayes River outcrop are suggestive of a possible correlation, though we do not have glass analyses of the rhyodacite to test this hypothesis.

Other Regional Tephras Possibly Correlated to Hayes Volcano

Several fine-grained, felsic distal tephras known informally as the Devil and Watana tephras are widespread in the Susitna Valley (fig. 1*A*) and have been described as having Hayes Volcano-like mineralogy and major-element glass composition (table 9, fig. 8; J.E. Dixon and others, written commun(s)., 1985; Dilley, 1988). The Watana tephra has a distinctive upper oxidized component and lower non-oxidized component in subaerial exposures, and as many as three discrete layers in a lake-sediment core. The tephra ranges in thickness from 6–20 cm, and has an age within the range of 2,830–5,270 ^{14}C yr B.P. based on radiocarbon ages of numerous paleosols bounding this layer in the Susitna River valley (J.E. Dixon and others, written commun(s)., 1985; Dilley, 1988). The Devil tephra is as much as 8 cm thick and is usually found directly beneath the surface organic mat (Dixon and Smith, 1990). The tephra was erupted between 1,516–1,420 ^{14}C yr B.P. (Dixon and Smith, 1990). Although the Devil and Watana tephras are difficult to distinguish from each other petrographically and geochemically (and thus are probably from the same source), they can be distinguished in the field on the basis of stratigraphic position, color, and texture. Attempts to correlate the Watana tephra to Hayes tephra set H of Riehle (1985 and 1994) are not conclusive due to the large spread in radiocarbon ages and limited geochemical data (J.E. Dixon and others, written commun(s)., 1985; Dilley, 1988; Dixon and Smith, 1990). We agree that the Watana and Devil tephras most likely erupted from Hayes Volcano and probably correlate to one or more tephras of tephra set H, but more work is needed to be conclusive. Finally, Riehle (1985) described a possible Hayes Volcano-like tephra located 110 km northeast of the vent (fig. 1*B*, site 27) with an approximate age of 500–1,000 ^{14}C yr B.P.

Possible Regional Correlatives to the Hayes River Ignimbrite

While it remains possible that the rhyodacite within Unit II correlates with the Oshetna tephra, thus far no tephras have been identified in the regional stratigraphic record that are correlative with the rhyolitic Hayes River ignimbrite, which has glass chemistry and mineralogy distinctive from other eruptive products from Hayes Volcano. No obvious Hayes River ignimbrite correlatives, comparing glass geochemistry or age (~40–30 ka), could be found in published records from unglaciated interior Alaska and northwestern Canada sediment sequences, although such records only document tephra deposits northeast of Hayes Volcano (Begét, 1996; Preece and others, 1999; Begét, 2001; Jensen and others, 2008; 2013; Preece and others 2011).

Concluding Remarks

The recognition of a possibly pre-Holocene age pyroclastic-flow deposit at the Hayes River outcrop, here informally named the Hayes River ignimbrite, indicates explosive eruptive activity of Hayes Volcano that predates the eruption of the well known late Holocene-age Hayes tephra set H. Previous assessments showed only that the volcano produced a series of explosive eruptions in the middle-to-late Holocene, and little is known about younger and older tephras apparently not correlative with Hayes tephra set H. The results of this study indicate additional complexity in the eruptive history of Hayes Volcano. We now also recognize that the volcano has produced dacitic, rhyodacitic, and rhyolitic magmas. Given the location of the vent area at ~11,000 ft above sea level in highly glaciated terrain, preservation of volcanic deposits that would reveal the pre-Holocene eruptive history is poor, at best. Records of other explosive eruptions of Pleistocene age are likely to be poorly preserved in this actively glaciated environment. Additional field work, both on the volcanic edifice and along surrounding drainages, coupled with radiometric dating and compositional correlation, would help to further elucidate the eruptive history of this little studied Alaskan volcano.

References Cited

Abdel-Rahman, A.-F.M., 1994, Nature of biotites from alkaline, calc-alkaline, and peraluminous magmas: Journal of Petrology, v. 35, p. 525–541.

Armstrong, J.T., 1995, CITZAF—A package of correction programs for the quantitative electron microbeam x-ray analysis of thick polished materials, thin films, and particles: Microbeam Analysis, v. 4, p. 177–200.

Begét, J.E., 2001, Continuous Late Quaternary proxy climate records from loess in Beringia: Quaternary Science Reviews, v. 20, no. 1, p. 499–507.

Begét, J.E., 1996, Tephrochronology and paleoclimatology of the last interglacial-glacial cycle recorded in Alaskan loess deposits: Quaternary International, v. 34, p. 121–126.

Begét, J.E., Campbell, K., Reger, R.D., Pinney, D., and Gillispie, T., 1991, Correlation of the Holocene Jarvis Creek, Tangle Lakes, Cantwell, and Hayes tephras in south-central and central Alaska: Quaternary Research, v. 35, no. 2, p. 174–189.

Birkeland, P.W., 1999, Soils and geomorphology (3rd ed.): Oxford, UK, Oxford University Press, 432 p.

Bowers, P. M., 1979, The Cantwell ash bed, a Holocene tephra in the central Alaska Range, Short Notes on Alaskan Geology, Alaska Division of Geological and Geophysical Surveys Geologic Report, v. 61, p. 19-24.

Child, J.K., Begét, J.E., and Werner, A., 1998, Three Holocene tephras identified in Lacustrine sediment cores from the Wonder Lake area, Denali National Park and Preserve, Alaska, U.S.A.: Arctic and Alpine Research, v. 30, p. 89–95.

Combellick, R.A., and Pinney, D.S., 1995, Radiocarbon age of probable Hayes tephra, Kenai Peninsula, Alaska *in* Combellick, R.A., and Tannian, F., eds., Short Notes on Alaskan Geology: Alaska Division of Geological and Geophysical Surveys Professional Report 117, p. 1–9.

de Fontaine, C.S., Kaufman, D.S., Anderson, R.S., Werner, A., Waythomas, C.F., and Brown, T.A., 2007, Late Quaternary distal tephra-fall deposits in lacustrine sediments, Kenai Peninsula, Alaska: Quaternary Research, v. 68, p. 64–78.

Dilley, T.E., 1988, Holocene tephra stratigraphy and pedogenesis in the middle Susitna River valley, Alaska: Fairbanks, University of Alaska, unpub. M.S. thesis, 97 p.

Dixon, E.J., and Smith, G.S., 1990, A regional application of tephrochronology in Alaska, *in* Lasca, N.P., and Donahue, J., eds., Archeological geology of North America: Boulder, Colo., Geological Society of America, Centennial Special Volume 4, p. 383–398.

Fierstein, J., 2007, Explosive eruptive record in the Katmai region, Alaska Peninsula: an overview, Bulletin of volcanology, v. 69, no. 5, p. 469-509.Fontana, M.R., 1988, Holocene tephrochronology of the Matanuska Valley, Alaska: Fairbanks, University of Alaska, unpub. M.S. thesis, 99 p.

Ghiorso, M.S., and B.W. Evans, 2008, Thermodynamics of rhombohedral oxide solid solutions and a revision of the Fe-Ti two-oxide geothermometer and oxygen-barometer, American Journal of Science, v. 308, p. 957–1039.

Hildreth, W., and Fierstein, J., 2012, Eruptive history of Mount Katmai, Alaska, Geosphere, v. 8, no. 6, p. 1527-1567.

Hildreth, W., and Fierstein, J. ,2000, Katmai volcanic cluster and the great eruption of 1912, Geological Society of America Bulletin, v. 112, no. 10, p. 1594-1620.

Jarosewich, E., Nelen, J.A., and Nordberg, J.A., 1979, Electron microprobe reference samples for standard analysis: Smithsonian Contributions to the Earth Sciences, v. 22, p. 68–72.

Jensen, B.J., Froese, D.G., Preece, S.J., Westgate, J.A., and Stachel, T., 2008, An extensive middle to late Pleistocene tephrochronologic record from east-central Alaska: Quaternary Science Reviews, v. 27, no. 3, p. 411–427.

Jensen, B.J., Reyes, A.V., Froese, D.G., and Stone, D.B., 2013, The Palisades is a key reference site for the middle Pleistocene of eastern Beringia—New evidence from paleomagnetics and regional tephrostratigraphy: Quaternary Science Reviews, v. 63, p. 91–108.

Johnson, D.M., Hooper, P.R., and Conrey, R.M., 1999, XRF analysis of rocks and minerals for major and trace elements on a single low dilution Li-tetraborate fused bead: Advances in X-ray Analysis, v. 41, p. 843–867.

Keith, M.L., and Weber, J.N., 1964, Carbon and oxygen isotopic composition of selected limestones and fossils: Geochimica et Cosmochimica Acta, v. 28, no. 10, p. 1787–1816.

Leake, B., Woolley, A., Birch, W., Burke, E., Ferraris, G., Grice, J., Hawthorne, F., Kisch, H., Krivovichev, V., Schumacher, J., Stephenson, N., and Whittaker, E., 2003, Nomenclature of amphiboles—Additions and revisions to the International Mineralogical Association's amphibole nomenclature: Canadian Mineralogist, v. 41, p. 1355–1370.

McHugh, K., Hart, W.K., and Coombs, M.L., 2012, Adakitic volcanism in the eastern Aleutian arc—Petrology and geochemistry of Hayes volcano, Cook Inlet, Alaska [abs.]: American Geophysical Union Fall Meeting, no.V31A–2760.

Miller, T.P., and Smith, R.L., 1976, "New" volcanoes in the Aleutian volcanic arc, *in* Cobb, E.H., ed., The United States Geological Survey in Alaska—Accomplishments during 1975: U.S. Geological Survey Circular 733, p. 11.

Pewe, T.L., 1975, Quaternary stratigraphic nomenclature in unglaciated central Alaska, U.S. Geologuca Survey Professional Paper 862.

Preece, S.J., Westgate, J.A., Froese, D.G., Pearce, N.J.G., and Perkins, W.T., 2011, A catalogue of late Cenozoic tephra beds in the Klondike goldfields and adjacent areas, Yukon Territory: Canadian Journal of Earth Sciences, v. 48, no. 10, p. 1386–1418.

Preece, S.J., Westgate, J.A., and Gorton, M.P., 1992, Compositional variation and provenance of late Cenozoic distal tephra beds, Fairbanks area, Alaska: Quaternary International, v. 13/14, p. 97–101.

Preece, S.J., Westgate, J.A., Stemper, B.A., and Péwé, T.L., 1999, Tephrochronology of late Cenozoic loess at Fairbanks, central Alaska: Geological Society of America Bulletin, v. 111, no. 1, p. 71–90.

Reimer P.J., Bard, E., Bayliss, A., Beck, J.W., Blackwell, P.G., Ramsey, C.B., Buck, C.E., Cheng, H., Edwards, R.L., Friedrich, M., Grootes, P.M., Guilderson, T.P., Haflidason, H., Hajdas, I., Hatté, C., Heaton, T.J., Hoffmann, D.L., Hogg, A.G., Hughen, K.A., Kaiser, K.F., Kromer, B., Manning, S.W., Niu, M., Reimer, R.W., Richards, D.A., Scott, E.M., Southon, J.R., Staff, R.A., Turney, C.S.M., Plicht, J.v.d., 2013, IntCal13 and Marine13 radiocarbon age calibration curves 0-50,000 years cal BP: Radiocarbon, v. 55, n. 4, p. 1869–87.

Riehle, J.R., 1985, A reconnaissance of the major Holocene tephra deposits in the upper Cook Inlet region, Alaska: Journal of Volcanology and Geothermal Research, v. 26, no. 1-2, p. 37–74.

Riehle, J.R., 1994, Heterogeneity, correlatives, and proposed stratigraphic nomenclature of Hayes tephra set H, Alaska: Quaternary Research, v. 41, no. 3, p. 285–288.

Riehle, J.R., Bowers, P.M., and Ager, T.A., 1990, The Hayes tephra deposits, an upper Holocene marker horizon in south-central Alaska: Quaternary Research, v. 33, no. 3, p. 276–290.

Schiff, C. J., Kaufman, D. S., Wallace, K. L., Werner, A., Ku, T. L., and Brown, T. A., 2008, Modeled tephra ages from lake sediments, base of Redoubt Volcano, Alaska, Quaternary Geochronology, v. 3, no.1, p. 56-67.

Stuiver, M., and Reimer, P.J., 1993, Extended 14C database and revised CALIB radiocarbon calibration program: Radiocarbon, v. 35, p. 215–230.

Vogel, J.S., Southon, J.R., Nelson, D.E., and Brown, T.A. , 1984, Performance of catalytically condensed carbon for use in accelerator mass spectrometry: Nuclear Instruments and Methods in Physics Research Section B–Beam Interactions with Materials and Atoms, v. 5, no. 2, p. 289–293.

Waitt, R.B., and Begét, J.E., 2009, Volcanic processes and geology of Augustine Volcano, Alaska, U.S. Geological Survey Professional Paper 1762, 78 p.

Waythomas, C.F., and Miller, T.P., 2002, Preliminary volcano-hazard assessment for Hayes volcano, Alaska: U.S. Geological Survey Open-File Report 02–072, 33 p.

White, J.D.L., and Houghton, B.F., 2006, Primary volcaniclastic rocks: Geology, v. 34, no. 8, p. 677–680.

Whitney, D.L., and Evans, B.W., 2010, Abbreviations for names of rock-forming minerals: American Mineralogist, v. 95, p. 185–187.

Menlo Park Publishing Service Center, California
Manuscript approved for publication on July 11, 2014
Edited by Chet Zenone and Katherine Jacques
Design and layout by Vivian Nguyen

ISSN 2328-0328 (online)
http://dx.doi.org/10.3133/sir20145133